

Citation for published version:

Awang Ngah, S, Dams, B, Ansell, M, Stewart, J, Hempstead, R & Ball, R 2020, 'Structural performance of fibrous plaster. Part 1: Physical and mechanical properties of hessian and glass fibre reinforced gypsum composites', *Construction and Building Materials*, vol. 259, 120396.
<https://doi.org/10.1016/j.conbuildmat.2020.120396>

DOI:

[10.1016/j.conbuildmat.2020.120396](https://doi.org/10.1016/j.conbuildmat.2020.120396)

Publication date:

2020

Document Version

Peer reviewed version

[Link to publication](#)

Publisher Rights

CC BY-NC-ND

University of Bath

Alternative formats

If you require this document in an alternative format, please contact:
openaccess@bath.ac.uk

General rights

Copyright and moral rights for the publications made accessible in the public portal are retained by the authors and/or other copyright owners and it is a condition of accessing publications that users recognise and abide by the legal requirements associated with these rights.

Take down policy

If you believe that this document breaches copyright please contact us providing details, and we will remove access to the work immediately and investigate your claim.

Structural Performance of Fibrous Plaster. Part 1: Physical and mechanical properties of hessian and glass fibre reinforced gypsum composites

Shamsiah Awang Ngah^{1,4,*}, Barrie Dams¹, Martin P Ansell¹, John Stewart², Russell Hempstead³, Richard J Ball¹

Address:

1. BRE Centre for Innovative Construction Materials, Department of Architecture and Civil Engineering, University of Bath, Bath BA2 7AY, UK

2. Historic England, 4th Floor, Cannon Bridge House, 25 Dowgate Hill, London EC1R 2YA, UK

3. Hayles and Howe, Templegate, Mead Rise, Bristol BS3 4RP, UK

4. Present address: Lightweight Manufacturing Centre, National Manufacturing Institute Scotland, University of Strathclyde, Block E, Westway Business Park, Porterfield Road, Renfrewshire, PA4 8DJ, UK

* Corresponding author: Email: sban20@bath.ac.uk

Abstract

Hessian fibre-reinforced gypsum, known as fibrous plaster, is a common material used for the manufacture of decorative features, including ceilings and walls in historic buildings, such as theatres and ballrooms, since the mid 19th century. It is still fabricated with modern materials for the decoration of new buildings in the UK, the Middle East and elsewhere. Following several recent failures of historic fibrous plaster ceilings in England, there is an urgent need to understand how these materials perform. There is no previous scientific investigation into the physical and mechanical properties of this material. As an initial experimental study, the microstructure of low and high density gypsum plaster were evaluated together with traditional hessian fabrics and modern glass fabrics, which are supplementing or replacing hessian fabrics. The chemical and physical characteristics were evaluated by X-ray diffraction, mercury intrusion porosimetry and dynamic vapour sorption. For the hessian, fibre density was measured and single filament strength measured to ascertain the effect of long-term ageing in new and historic material. Flexural tests were performed on gypsum plaster reinforced with different configurations of hessian and glass fabric reinforcements. Single filaments from historic hessian were weaker than filaments from new hessian and the larger scatter in strength was demonstrated using a

Weibull distribution function. High density gypsum absorbed less moisture (0.2%) than low density gypsum (1%), as expected, but the jute fibres in the hessian absorbed more than 20% of the moisture. High density gypsum was considerably stronger than low density material, and random glass mats as reinforcement resulted in the highest flexural strengths and ability to yield to higher strains, due to enhanced interfacial bonding. This work will have high impact by providing a much needed basis for understanding the long-term degradation of fibrous plaster systems.

Keywords:

Fibrous Gypsum Plaster; Jute Fibres; Glass fibres; Sorption and Desorption Isotherms; Mercury Intrusion Porosimetry (MIP); Flexural Strength; Single Fibre Tensile Strength; Microstructure

1. Introduction

Ornamental plasterwork is a common feature of historic buildings, in the form of ceilings, cornices and mouldings. Until the 19th century, it was made of lime mortar and hair, or plaster of Paris (gypsum). The search for cheaper ornamentation led to the development of fibrous plaster, a natural fibre composite material composed of gypsum plaster as the matrix and reinforced with hessian scrim and timber. This method was first introduced in the UK by the Frenchman Leonard Alexander Desachy, which he successfully patented in 1856 [1]. By the early 20th century, fibrous plaster had become ubiquitous in higher status buildings [2] as an economical and efficient alternative to traditional lime plaster. In addition to being relatively lightweight, it could be fabricated off-site, during construction of the building. Figure 1 shows a few examples of decorative fibrous plasterwork which can be seen in buildings across the UK.

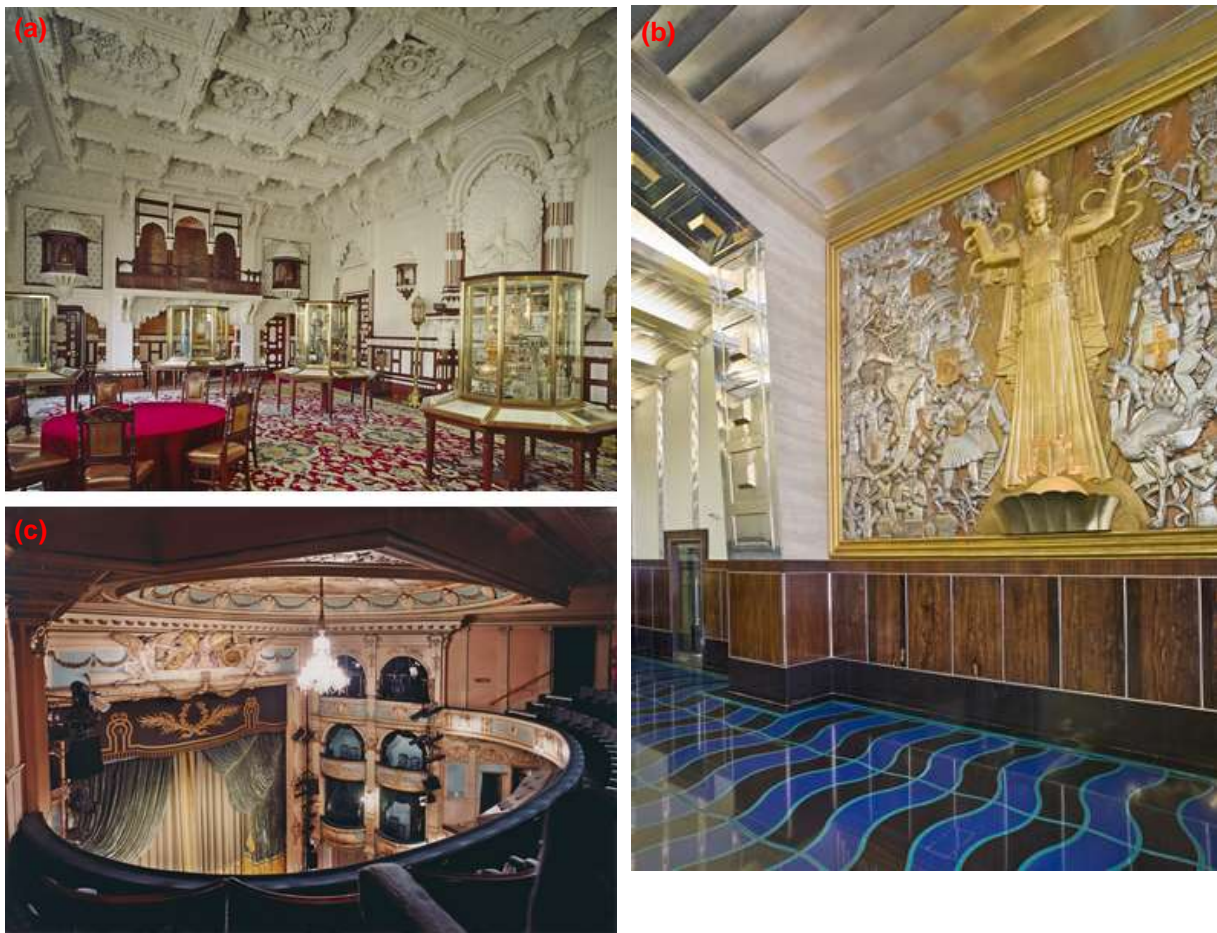


Figure 1: Decorative fibrous plaster ceiling in buildings across the UK. (a) Durbar Room, Osborne House, Isle of Wight, 1891 (b) Former Daily Express Building, London, 1932 (c) Wyndham's Theatre, London, 1899 (All images © Historic England Archive)

There have undoubtedly been occasional failures of fibrous plaster ceilings from time-to-time, as with ceilings of lime plaster and timber lath. However, from 2013 there were several

major collapses involving fibrous plaster ceilings in public buildings, raising concerns for their structural integrity [3]. The most serious incident was at the Apollo Theatre, London, in 2013, where a large part of the ceiling of the 112 year-old building collapsed during a performance. This resulted in the injury of 88 members of the audience. A few more examples of similar incidents occurred at the Empress Ballroom, Blackpool in September, 2017 [4] and the Savoy Hotel, London in March, 2019 [5], in which the collapse was attributed to several factors ranging from failure of wads without wire, natural ageing or bio-deterioration of hessian reinforcement to overloading of the ceiling with various infrastructures. These incidents have prompted the theatre industry, the Health & Safety Executive and other bodies to raise standards in ceiling inspection. This also led Historic England (the government agency responsible for the historic built environment in England), to initiate a wide-ranging investigation into fibrous plasterwork, in order to better understand the history, deterioration, assessment and repair of the material [1]. Historic fibrous plaster had been completely neglected in scientific research, unlike other materials such as the deterioration of stone masonry. These investigations are the first in a series to characterise this composite material.

Traditional materials in the fabrication of fibrous plaster panels include Plaster of Paris (deriving its name from initial imports of the material into England from quarries near Paris in the Middle Ages) also known as casting plaster and hessian scrim as the reinforcement, both within a timber framework.

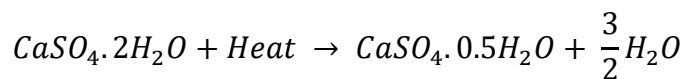
The main constituent in Plaster of Paris is calcium sulphate hemihydrate ($CaSO_4 \cdot 0.5H_2O$). Generally, gypsum plaster consists of three different phases of chemicals namely calcium sulphate dihydrate ($CaSO_4 \cdot 2H_2O$), calcium sulphate hemihydrate ($CaSO_4 \cdot 0.5H_2O$) and calcium sulphate anhydrite ($CaSO_4$), in which the ratio of these chemicals determines the chemical, physical and mechanical properties of the resulting gypsum plaster [6]. For clarification, gypsum is the name of the raw material while gypsum plaster refers to the processed and hydrated gypsum powder [6].

Calcium sulphate hemihydrate (CSH) normally exists in two forms, depending on the calcining method used during the production stage. Calcining is a process of chemical change through heating where raw gypsum, calcium sulphate dihydrate ($CaSO_4 \cdot 2H_2O$) is converted to CSH ($CaSO_4 \cdot 0.5H_2O$) by removing 1.5 water molecules. Traditional calcination involved heating gypsum in a kiln, resulting in beta plaster (β -CSH); nowadays it is produced via a dry calcining

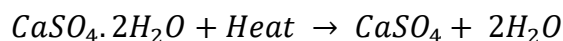
method utilising a rotary kiln at atmospheric pressure and temperature between 120 and 180°C [7], which results in fragmentary gypsum crystals [6]. The modern variation, produced since the 1930's, makes alpha plaster (α -CSH) by wet calcining in a high pressurised steam autoclave at a temperature between 80°C and 150°C [7]. This creates a compact and even crystalline gypsum structure [6].

Calcined gypsum (both α - and β -CSH) can be reverted to original dihydrate gypsum through hydration. Hydration of CSH is a highly exothermic reaction, which occurs rapidly after mixing with water. The chemical reactions for both calcination and hydration processes are described in Equation 1 and Equation 2 respectively [7]. As shown in these equations, calcium sulphate dihydrate is both the starting material before calcining as well as the final product after hydration. Both α - and β -CSH differ in their reactivity with water and in the strength of the hydration products [8]. For instance, β -CSH requires more water and sets more rapidly, therefore is lower in strength when compared to α -CSH.

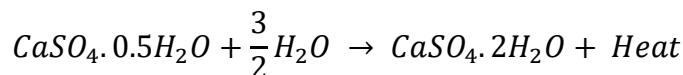
Calcination Process:



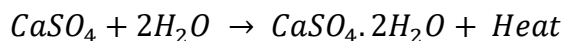
Equation 1



Hydration Process:



Equation 2



It has been reported that beta plaster was used exclusively until the Second World War [1]. On the other hand, alpha plaster was invented in the 1930s and became the material of choice for the manufacture of new fibrous plaster by the end of the century, due to its higher strength. In conservation work, no standardised material is specified as different plastering manufacturers currently use the traditional or modern system for repairs, according to their perceptions of its benefits.

Cast gypsum was commonly used for small cast ornaments, applied to the surface of walls and ceilings. Casting pure gypsum plaster for large structures without reinforcement was not practical, as gypsum is well-known for its brittleness, weakness in tension and low impact

strength, in addition to its high water solubility [9]. These undesirable properties would likely cause severe damage to the cast structure when subject to applied loads. Combining fibres with gypsum reduces its brittleness appreciably and improves its mechanical properties, especially the post-cracking behaviour [10]. The invention of fibrous plaster allowed gypsum to be used in an entirely different manner for decoration.

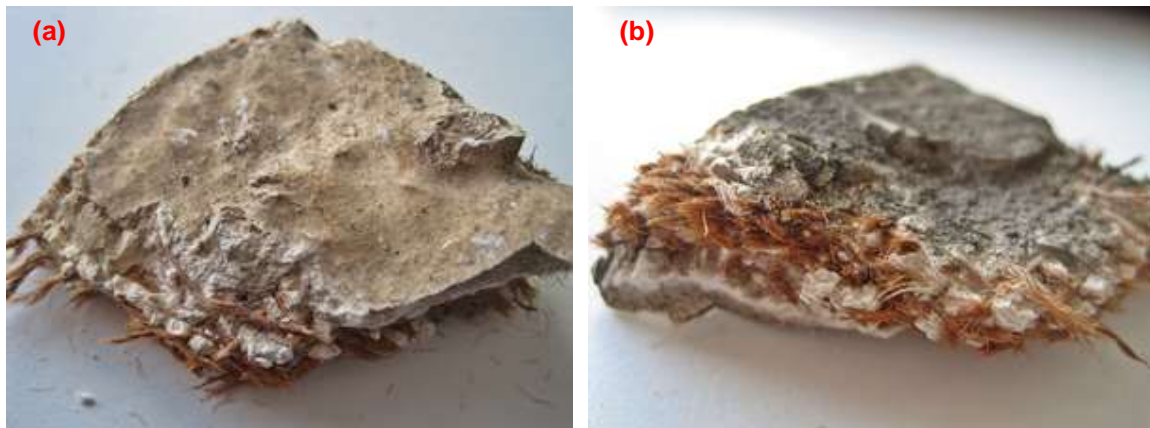


Figure 2 : Appearance of historic fibrous plaster containing hessian scrim (a) exposed painted surface (underside), (b) surface in roof space (top side).

Hessian (jute or hemp) has been used as a reinforcement for fibrous plaster in the UK for well over 100 years. Figure 2 shows some sections of historic fibrous plaster where hessian scrim comprising bundle of fibres, were embedded in gypsum plaster as illustrated in Figure 3(a). Figure 3(c) shows the formation of gypsum microstructure when observed under electron microscope. Jute and hemp are among bast fibres that possess a higher cellulose content, with a smaller microfibril angle (orientation angle) compared to other fibres such as coir [11]. Bast fibres are extracted from the outer part of plant stems by a retting process in which the whole plant stems are immersed in water and the separation process is accomplished by means of biological or chemical degradation [12]. The morphology of jute fibres is shown in Figure 3b. India, China and Bangladesh are the largest producers of jute fibres [13]. However, the main concern in the use of natural fibres as the reinforcement is the poor interfacial adhesion between fibres and matrix which is likely to affect its mechanical performance [11], and its susceptibility to biodeterioration.

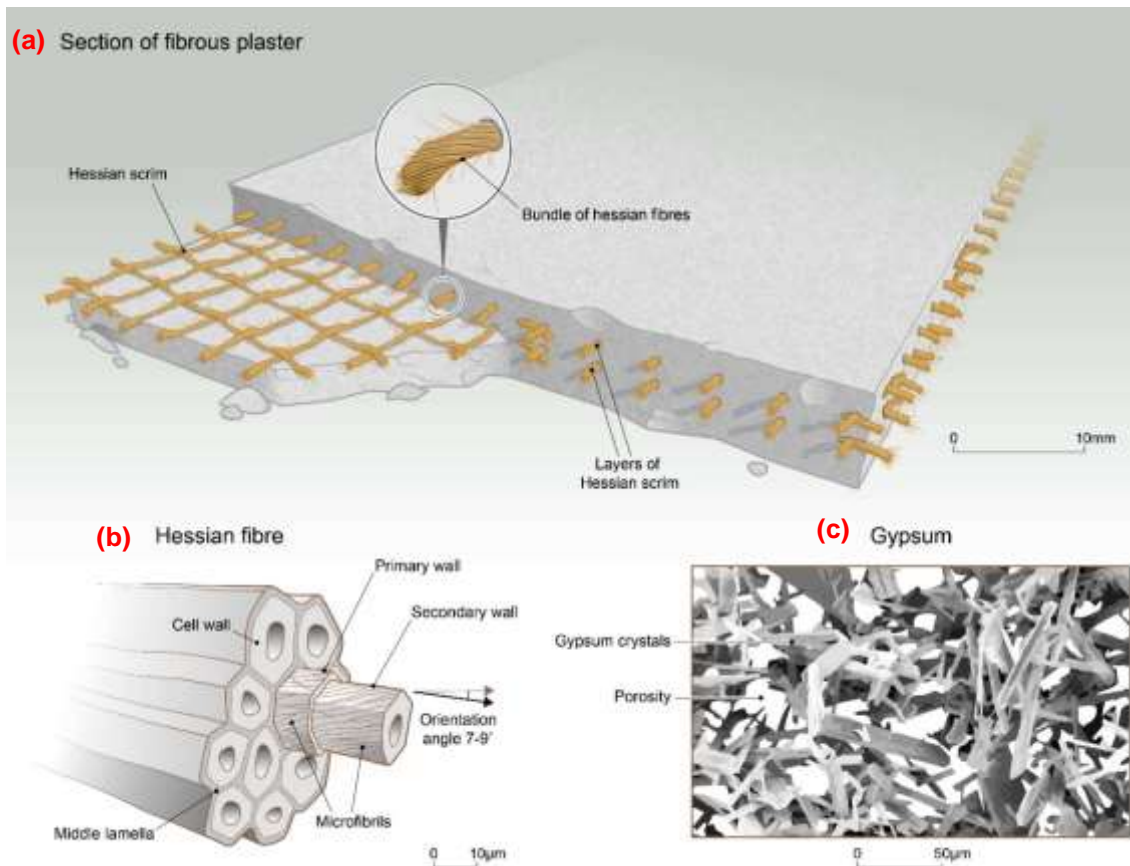


Figure 3 : Fibrous plaster illustration. (a) Section of fibrous plaster with exposed scrim layer (b) Hessian (Jute) fibre morphology – each fibre is comprised of a bundle of ultimate fibres; (c) Gypsum crystal microstructure

88

89 Besides hessian (jute) fibres, some companies making modern fibrous plaster [14, 15]
 90 now use glass fibre mat as a substitute for hessian, since it is stronger and exhibits a much
 91 higher modulus of elasticity and strength. This produces thin and lightweight panels of glass
 92 fibre-reinforced gypsum (GFRG), now found in applications including 3D wall panels and
 93 column casings as well as ceiling panels [14]. Besides being a versatile and robust material
 94 with a high degree of impact resistance, GFRG is also resistant to biodeterioration and is highly
 95 flame resistant, due to the nature of gypsum, which acts like a thermal regulator when exposed
 96 to a flame. Not only will it not burn, but it is also capable of protecting the materials behind from
 97 the heat of the flame for up to two hours [15]. In addition, several studies [9, 16] have
 98 demonstrated that GFRGs exhibit enhanced toughness and energy dissipation capacity.

99 In the interest of using eco-friendly materials, some researchers have reinforced gypsum
 100 with abaca fibres [10] and bio-degummed hemp fibres [17], both of which had been surface-
 101 treated in order to improve the mechanical properties and thermal resistance of resulting
 102 composites. There have also been studies that investigated the microstructural and mechanical

behaviour of gypsum reinforced with polyamide fibres [18] as well as the influence of hydrophilic polyvinyl alcohol (PVA) fibres and hydrophobic polypropylene (PP) fibres on the physical and mechanical properties of gypsum composites [19]

The aims of the present work were to investigate the structural performance of fibrous plaster; to study the most effective material combinations for new fibrous plaster potentially used in restoration; and to support the wide-ranging investigation of Historic England into structural failures. As there has been no published investigation into these materials previously, the fundamental properties of gypsums as individual materials and in combination with hessian and glass fibre reinforcements will provide a much needed insight into the behaviour of fibrous plaster composites in current and historic use. This investigation is particularly important to help academia and industry understand their performance in buildings and to address the real-life concerns relating to maintenance and safety. In this paper, the results of mechanical testing of flat rectangular fibrous plaster panels containing different volume fractions of hessian or glass fibre mat are reported. The failure mechanism of the panels and the crystallisation of gypsum during hydration were examined and evaluated from electron microscopy images.

2. Materials and Experimental Work

2.1 Materials

The materials in the present work were purchased from Industrial Plasters Ltd, Wiltshire, UK by Hayles and Howe, Bristol, UK. Two types of commercially available gypsum plasters were used, identified as alpha plaster (Prestia Creation) and beta plaster (Prestia Classic). Prestia Creation is a high strength plaster with low expansion rate and commonly used with fibreglass chopped strand mat or fibreglass mat while Prestia Classic is a standard casting plaster with faster setting time and extra durability. These materials are mainly comprised of calcium sulphate hemihydrate (CSH).

Alpha plaster (α -CSH) and beta plaster (β -CSH) differ in their reactivity with water and in the strength of the hydration products.[8, 20]. β -CSH requires more water than the α -CSH, in order to obtain a standard paste consistency as it has a much higher specific surface area [8]. In terms of microstructure, the α -CSH consists of well-formed transparent idiomorphic crystals with sharp crystal edges whereas β -CSH consists of flaky particles made up of small crystals [8]. The properties of these gypsum plasters are listed in Table 1. Their chemical and

mineralogical composition was assessed by X-ray diffraction analysis (XRD) and is reported in Section 2.3.1.

Table 1 : Properties of gypsum plaster

Properties	Alpha Plaster (α -CSH) [21]	Beta Plaster (β -CSH) [22]
Plaster /Water Ratio	100/48 to 55	100/66 to 77
Working time (min)	12	10
Demould time (min)	25-30	25-35
Expansion (%)	0.15	0.10
Compressive Strength (MPa)	25	13

Two different types of reinforcement, as shown in Figure 4, were used to manufacture samples of fibrous plaster, namely hessian (a, b) and glass fibre (c,d). The hessian fabric was made of jute fibres imported from India. Two different weave styles were investigated, a loose plain weave with an average mesh of 5 mm x 10 mm and a tighter plain weave with an average mesh of 2.9 x 3.4 mm. The glass fibre reinforcements used were a 225 gsm Unifilo U816 CFM Fibreglass Mat [23] and a 185 gsm quadaxial glass [24]. CFM consists of randomly oriented strands in multiple layers, held together with a binder, while the quadaxial glass is a multiaxial glass reinforcement, constructed like a lace consisting of four layers of E-glass fibres aligned in 0°/-45°/90°/+45° orientations and stitched together with the fire-proof aramid material Nomex [25].



Figure 4: Type of reinforcements. Traditional hessian fabric - (a) Loose weave hessian and (b) Plain weave hessian; Modern glass fabric - (c) Continuous fibreglass mat (CFM) and (d) Quadaxial glass fabric

Plaster retarder was also added to certain formulations in order to control and delay the setting time. Two types of plaster retarder were used, sodium citrate and pearl glue, each type weighing approximately 5 grams. These retarders were mixed with approximately 3.5 litre water in a 3 gallon sized bucket prior to adding gypsum plaster until the mixture reached the required consistency. For pearl glue retarder, the liquid mixture was then boiled,hydrated lime was added and finally the mixture was sieved to remove lumps.

2.2 Manufacture of fibrous plaster

Flat rectangular specimens of fibrous plaster were manufactured by Hayles and Howes following the configuration described in Table 2. This was to compare properties of fibrous material made with traditional and modern materials.

Table 2 : Flexural sample configurations

No	Gypsum Plaster	Retarding Agent	Reinforcement	Reinforcement Layer	Sample ID
1	Beta	-	-	No reinforcement	B-Gypsum
2	Beta	-	H-LW	1	B+1H-LW
3	Beta	-	H-LW	2	B+2H-LW
4	Beta	-	H-LW	3	B+3H-LW
5	Beta	-	H-PW	2	B+2H-PW
6	Alpha	-	-	No reinforcement	A-Gypsum
7	Alpha	-	H-LW	2	A+2H-LW
8	Beta	R	H-LW	2	B_R+2H-LW
9	Beta	RGS	H-LW	2	B_RGS+2H-LW
10	Beta	-	GF-CFM	2	B+2GF-CFM
11	Beta	-	GF-QA	2	B+2GF-QA

Abbreviation:

Alpha: High strength plaster

Beta: Standard casting plaster

H-LW : Loose Weave Hessian Fabric

H-PW : Plain Weave Hessian Fabric

GF-CFM : Continuous Fibreglass Mat

GF-QA : Quadaxial Glass Fibre Fabric

R : Retarding agent - Sodium citrate

RGS : Retarding agent - Pearl glue

The manufacture of fibrous plaster was achieved by laying up the wet plaster and fabrics in a silicone rubber mould (see Figure 5) containing 12 recesses measuring 160 mm long by 40 mm wide by 6 mm deep. A film of soapy water was used as a release agent brushed onto the mould surface. Plaster was added to water in the ratio 140 parts plaster to 100 parts water and mixed to an even consistency. A mild exothermic reaction occurred but the thin specimens cooled quickly. The specimens were left to hydrate for 30 minutes before labelling with a felt tip pen, careful removal from the mould and packing into a bespoke wooden tray.



Figure 5 : Manufacture of fibrous plaster specimens showing (a) plaster in a silicone mould and (b) plaster and glass reinforcement materials used in the process

2.3 Chemical and Physical Characterisation of Gypsum and Reinforcement Materials

2.3.1 X-Ray Diffraction (XRD)

Phase purity and crystal structures of gypsum plasters were determined at room temperature by using x-ray powder diffraction in flat-sample transmission mode, using a STOE STADI P diffractometer equipped with MYTHEN detectors. The equipment was operated with Cu-K α 1 radiation ($\lambda = 1.540562 \text{ \AA}$) at a scanning rate of 3.67 degree per minute and a scanning 2θ range of 0° to 80°

Both hemihydrate ('as received' powder) and dihydrate gypsums obtained from flexural specimens were analysed. The dihydrate samples were ground into fine powder using a pestle and mortar. Samples were placed between two foils for insertion into the powder XRD chamber.

The analysis was also carried out to differentiate the mineralogical composition of α and β gypsum plasters.

2.3.2 Mercury Intrusion Porosimetry

MIP tests were performed on dihydrate gypsums taken from flexural specimens using Pascal 140 and Pascal 440, Thermo Fisher Scientific mercury porosimeters. The measurement was performed in two steps : first, the samples were intruded to 400 kPa in the Pascal 140 and then moved to the Pascal 440 where intrusion was from atmospheric pressure to a maximum pressure of 400 MPa; it was followed by extrusion back to atmospheric pressure again. This

intrusion-extrusion cycle in the low and high pressure porosimeter was performed twice for the alpha plaster and once for the beta plaster.

The mercury surface tension and contact angle between the mercury and the solid surface were taken as 480 mN/m and 140° respectively. A blank run for differential mercury compression was made to correct the volume measurements. The mercury intrusion volumes and the corresponding applied pressures were recorded at every pressure step and provide the basic data for the analysis of pore structure. The pore diameters related to the pressure applied can be calculated using the Washburn equation [26] based on the assumption that all pores are of a cylindrical shape.

2.3.3 Sorption and desorption isotherms via DVS

The sorption and desorption isotherm measurements on dihydrate gypsums and jute fibres were performed using a dynamic vapour sorption instrument (DVS Intrinsic from Surface Measurement Systems Ltd.). The instrument rapidly measures uptake and loss of moisture gravimetrically using a high precision balance with a resolution of 0.1 µg [27]. Prior to the test, all samples were dried in an oven at 60°C. The samples were placed in a temperature controlled chamber and exposed to a flowing carrier gas (air) at a specified relative humidity (RH). An air temperature of 23°C and a range of RH from 0-95% were chosen as the testing condition. During the measurements, the instrument was run in mass variation over time variation ($\frac{dm}{dt}$) mode which allows the software to determine when equilibrium has been reached to complete a relative humidity step.

2.4 Mechanical Characterisation of Reinforcement Material and Fibrous plaster

2.4.1 Fibre Density Measurement

The density of jute fibres was measured according to BS ISO 10119 Method A (liquid-displacement) [28] using an Ohaus density determination kit. Prior to the measurements, hessian scrim was dried in an oven at 60 °C. The jutes fibres were then separated and tied into bundles of fibres (Figure 6) and weighed in air and liquid to the nearest 0.0001 g. In order to remove air bubbles adhered to the surface and to ensure small lumens in the fibre structure filled up with immersion liquid, the submerged specimen was placed in a vacuum oven at 100 kPa for 20 minutes. The density of the fibres, ρ_f was calculated using Equation 3.

$$\rho_f = \left(\frac{w_a}{w_a - w_l} \right) \times \rho_l \quad \text{Equation 3}$$

where w_a is the weight of the specimen in air, w_l is the weight of the specimen in liquid and ρ_l is the density of the immersion liquid.

A store-bought canola oil was selected as the immersion liquid and its density was determined using a pycnometer method according to BS EN ISO 1675:1998 [29].



Figure 6 : Tied jute fibre bundles

2.4.2 Single Fibre Tensile Test

Tensile tests were performed on single fibre filaments as per BS ISO 11156 [30] on an Instron 3369 with a 50 N load cell at a crosshead speed of 1 mm/min. Specimens were prepared by gently separating individual fibre bundles from jute strands and mounting onto a cardboard sample holder at both ends, using a quick drying adhesive as shown in Figure 7(a). For each individual fibre bundle, the mass was weighed up to 5 decimal places and the length was measured as accurately as possible. The cross-sectional area of the single fibre was calculated using Equation 4.

$$A = \frac{m}{\rho_f \times l} \quad \text{Equation 4}$$

where A is the single fibre bundle cross-sectional area, m is the mass of a single fibre bundle at a given length, l is the length of the fibre bundle and ρ_f is the fibre bundle density.

The cardboard sample holder, which has a 25 mm gauge length slot in the middle, was then placed between pneumatic test grips ensuring the specimen was aligned with the loading axis of the test machine (Figure 7(b)). Before applying the load, the supporting sides of the

cardboard was cut in the middle at both sides to make sure only the fibre was under load during the test. Three grades of jute fibres, taken from historic hessian, new loose weave hessian and plain weave hessian, were tested. A minimum of twenty measurements were conducted for each type of fibre tested.

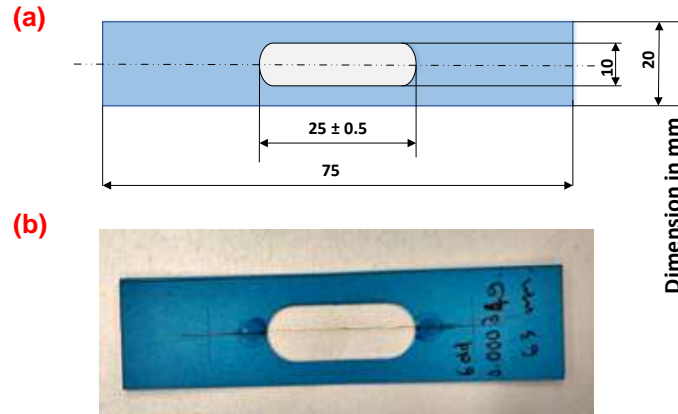


Figure 7 : Single Fibre Filament Test. (a) Mounting card dimension (b) Fibre mounted on cardboard

The 2-parameter Weibull probability distribution [31] was used to determine the cumulative distribution function of the jute fibres strength. The cumulative probability of failure (P_f) is defined as per Equation 5.

$$P_f = 1 - \exp \left[- \left(\frac{\sigma_f}{\sigma_o} \right)^m \right] \quad \text{Equation 5}$$

where σ_f is the single fibre tensile strength, σ_o is the scale parameter (i.e. characteristic strength) and m is the shape parameter (i.e. Weibull modulus), which indicates the distribution in fibre strength. Taking logarithms twice on both sides of Equation 5 results in Equation 6,

$$\ln \left[\ln \left(\frac{1}{1 - P_f} \right) \right] = m \ln \sigma_f + m \ln \sigma_o \quad \text{Equation 6}$$

The scale and shape parameter can be estimated by fitting the experimental data to Equation 6 which represents a linear function $\ln(\sigma_f)$ with the slope equal to m and the intercept equal to $m \ln(\sigma_o)$.

2.4.3 Flexural Tests

Flexural tests were carried out in accordance with BS EN ISO 178 [32] using an Instron 3366 universal testing machine with a 50 kN load cell at a crosshead speed of 2 mm/min. The flexural properties were measured in three-point bending with a span length to thickness ratio greater than 16:1. Rectangular specimens with dimensions of 160 mm x 40 mm x 6 mm thickness were tested until failure. The specimens had a smooth face and a rougher face from which some fibrous material was visible. With the fibres closer to the rough face, this surface was treated as the soffit with the fibres acting in tension. At least eight specimens were tested for most of the sample categories.

The samples were stored in the laboratory environment at room temperature (~22°C) and relative humidity of ~50% for two weeks allowing them all to reach an equilibrium prior to testing.

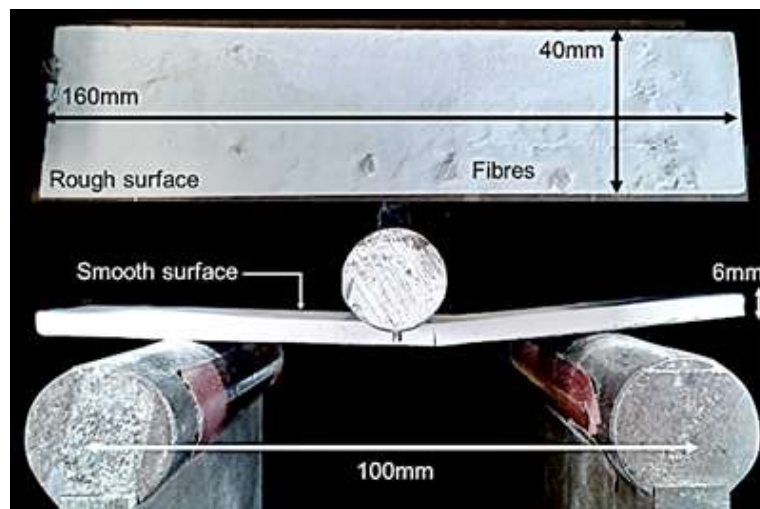


Figure 8 : Flexural test-setup

2.5 Microscopy Analysis

Samples were taken from cast sheets of alpha and beta gypsum plaster. The appearance of the white gypsum sheets was similar. Small samples were broken away from the cast sheets in order to present a clean fractured surface. Samples were mounted on conductive carbon adhesive discs on an aluminium stub. Both the surface of the cast sheet and the fractured surface were imaged.

Samples were sputter coated with a thin layer of gold for two minutes in an argon plasma at a voltage of 25kV. Samples were imaged in a JEOL JSM-6480LV SEM under an accelerating voltage of 20kV and a working distance of approximately 15 mm.

3. Results and Discussion

3.1 Classification of raw gypsum plasters

The raw material gypsums used in the present work identified as α -CSH and β -CSH differ in their reactivity with water and in the strength of the hydration products.[8, 20]. β -CSH requires more water than the α -CSH, in order to obtain a standard paste consistency as it has a much higher specific surface area.[8]. In terms of microstructure, the α -CSH consists of well-formed transparent idiomorphic crystals with sharp crystal edges whereas β -CSH consists of flaky particles made up of small crystals [8].

3.2 XRD Analysis

Figure 9 shows the XRD results of both hemihydrate and dihydrate gypsum plasters. The analysis shows a high-peak to background ratio indicating the samples are highly crystalline. The peaks are identified by comparing the present results with the XRD pattern published in previous studies [10, 33]. As expected, the XRD patterns reported in Figure 9 (a and b) showed peaks ascribed to calcium sulfate hemihydrate, anhydrite and calcite. The XRD patterns reported in Figure 9 (c and d) were mainly calcium sulfate dihydrate and a very small amounts of secondary constituents such as quartz. No peaks related to calcite were detected in the present study unlike XRD spectra previously published [33].

The XRD patterns also revealed that in general, the alpha and beta gypsum plasters have almost identical spectra suggesting the materials do not vary much in chemical composition. This is in accordance with a previous study, [33] which showed no observable differences in peak position but slight differences in relative intensity were removed when the α -hemihydrate was finely ground [20].

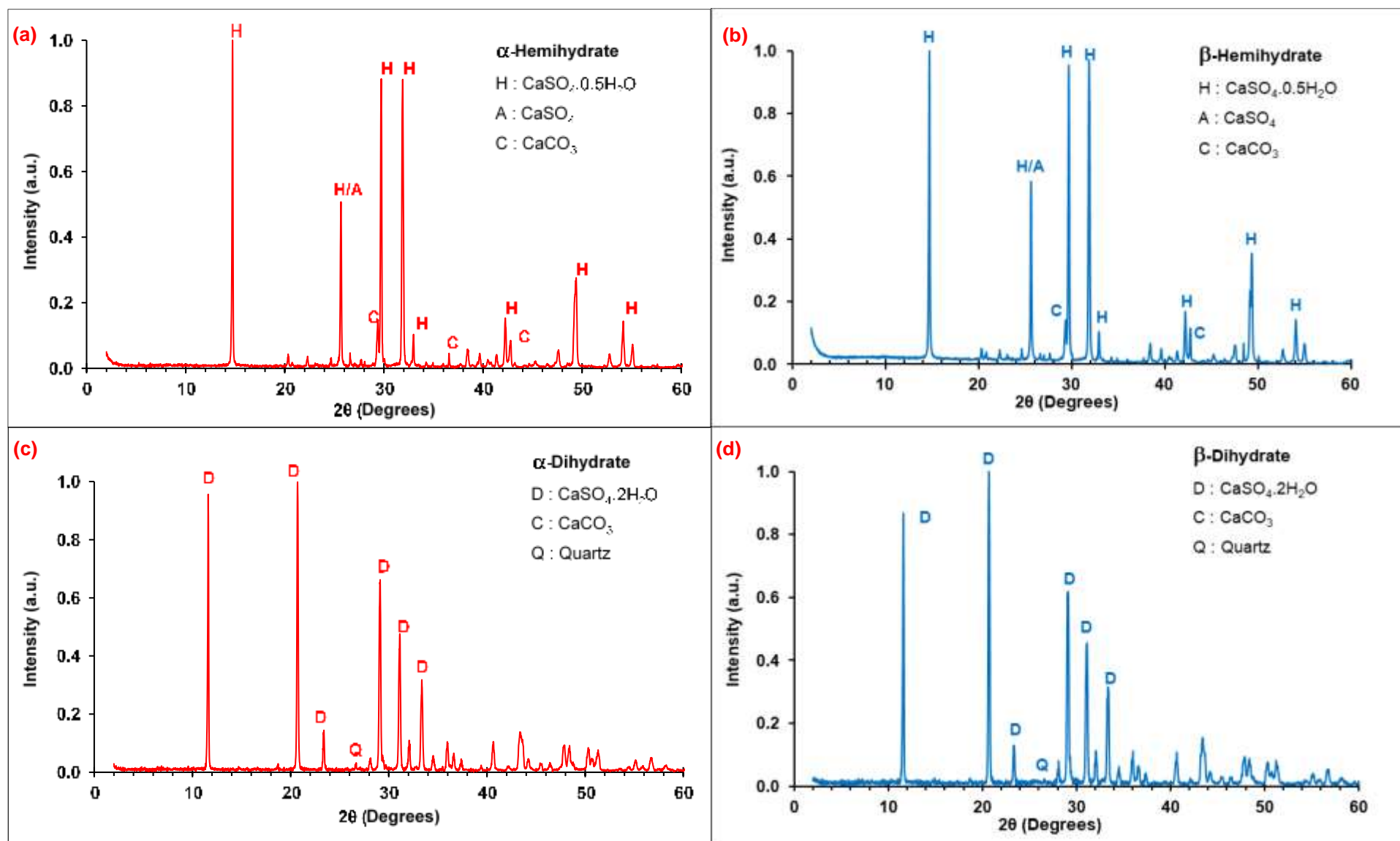


Figure 9 : XRD pattern for Gypsum Hemihydrate (a, b) and Gypsum Dihydrate (c, d)

3.3 Mercury Intrusion Porosimetry (MIP)

Mercury intrusion porosimetry is a technique which provides quantitative representation of the microstructure of porous materials from which pore size distribution can be deduced [34]. The technique is based on the gradual intrusion of a non-wetting liquid mercury into an evacuated pore system in the presence of external applied pressures [35]. The diameter of the pores intruded by mercury is inversely proportional to the applied pressure; the higher the pressure applied, the smaller are the pores which are being intruded. The volume of mercury required to fill all accessible pores is considered the total pore volume. The cumulative intruded volume curve and differential distribution curve for both alpha and beta gypsum dihydrate are shown in Figure 10.

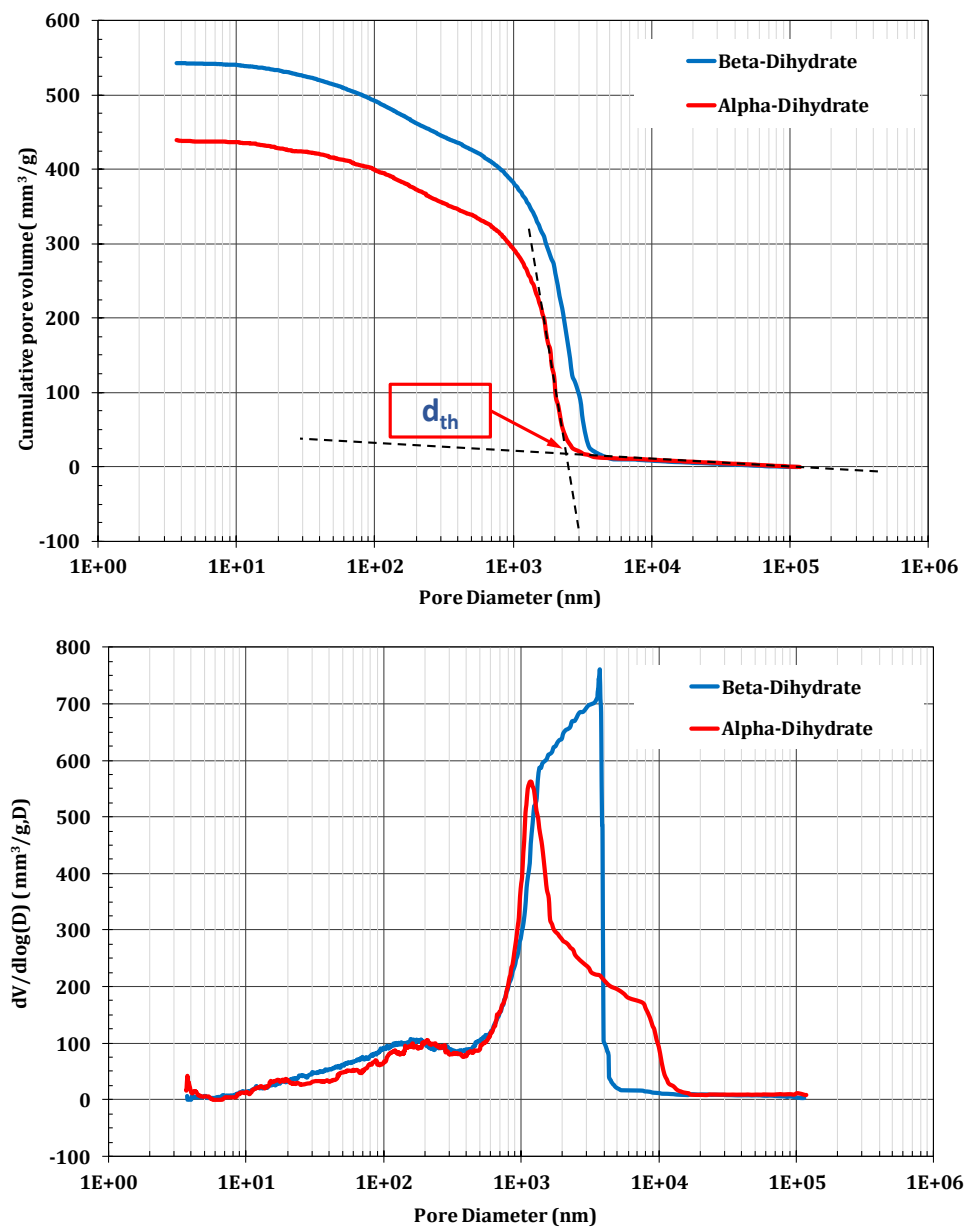


Figure 10 : Mercury Intrusion Curve of Gypsum Dihydrate. (a) Cumulative intruded volume curve
(b) Differential distribution curve

The key parameters derived from these curves can be used to evaluate the pore structure of the gypsum as listed in Table 3. The intrudable porosity, ϕ_{in} is obtained by taking the highest point on the cumulative intruded volume curve which corresponds to the smallest equivalent pore diameter, d_{min} . [36]. The critical pore diameter, d_{crit} is determined by taking the diameter which corresponds to the maximum peak in the differential distribution curve [36]. It is defined as the pore diameter above which no connected path could form throughout the sample [37]. It is well accepted that the smaller the critical pore diameter, the finer the pore structure. The threshold pore diameter, d_{th} is taken as the intersections of tangent lines on the cumulative intruded volume curve [38]. The threshold pore size is the size of pores providing entry to the pore network, i.e. connectivity, and it is one of the parameters controlling its transport properties [39]. Some studies [40] have taken the threshold diameter and the total volume of intruded mercury as indexes of the pore structure for comparison with pore structures of other materials. Both parameters vary with water-binder ratio and age in the same way with time.

Table 3 : MIP test results for Gypsum Dihydrate

Properties	β -Dihydrate	α -Dihydrate
Intrudable porosity, ϕ_{in} (mm ³ /g)	543	440
Minimum pore diameter, d_{min} (nm)	3.70	3.68
Critical pore diameter, d_{crit} (nm)	3714	1167
Threshold pore diameter, d_{th} (nm)	3670	2478
Average Pore Diameter, d_{avg} (nm)	230	195
Porosity (%)	58	52

It can be concluded from the MIP results that the beta gypsum contains a higher amount of pores (i.e. porosity) and larger threshold pore size indicating the gypsum has coarser pore structure when compared to the alpha gypsum. Therefore it is expected that the beta gypsum will exhibit lower material strength than the alpha gypsum. However, it should be noted that intrudable porosity as measured in MIP is not a measure of total porosity in the system [40]

3.4 Sorption and desorption isotherms via DVS

The sorption and desorption isotherms measured via DVS provide information on the hygroscopic behaviour of building materials such as gypsum. It relates the amount of equilibrium moisture content to the ambient relative humidity (RH) for a given temperature [41]. Hygroscopic materials constantly absorb and desorb moisture to and from the surface until equilibrium conditions are reached. Moisture penetrates the structure either in the form of liquid or vapour but only escapes in the vapour phase.[42].

Figure 11 displays the sorption and desorption isotherm curves for gypsum dihydrate and jute fibre. These curves are sigmoidal with marked hysteresis and exhibit a Type II (for jute fibre) and Type III (for gypsum) adsorption according to the IUPAC's classification [43]. Referring to Figure 11(a), the results indicate the different sorption properties between the alpha and beta gypsum plasters. The alpha gypsum shows a very low moisture uptake. The maximum uptake at 95% RH is around 0.20 wt %. In contrast, the beta gypsum exhibit higher water uptake i.e. 1.04% at 95% RH. The result agrees well with the fact that the beta gypsum has higher porosity and larger threshold pore size as determined from MIP analysis. It can also be seen from the graph that the desorption phase of both gypsums coincides with the sorption phase which indicates that the gypsum sorption and desorption processes are reversible.

The corresponding isotherm plot for jute fibre (Figure 11(b)) exhibits type II behaviour which is characterised by low initial sorption and substantial uptake at higher RH. It can be seen that the fibre takes up fairly large amount of moisture during the sorption phase. The weight increased by 21 % at 95 % RH. This is not surprising owing to the hydrophilic nature of plant fibres resulting from the presence of hydroxyl groups (OH) of anhydroglucose repeating units in the cellulose structure [44]. This leads to high level of moisture absorption from the surrounding environment especially in humid conditions. One of the main factors that influence the sorption and desorption behaviour of plant fibres is thought to be their chemical composition which comprises cellulose, hemicellulose and lignin. It was demonstrated that fibres with high lignin levels and relatively lower cellulose content such as jute, coir and Stika spruce exhibited higher moisture uptake compared to fibres having very low lignin level and relatively higher cellulose content such as cotton, flax and hemp [45]. For comparison, cotton fibre has the highest amount of cellulose (94% cellulose, 0% lignin) while coir fibre has the highest amount of

lignin (approximately 43% cellulose, 45% lignin). Jute fibre has approximately 72% cellulose and 13% lignin.

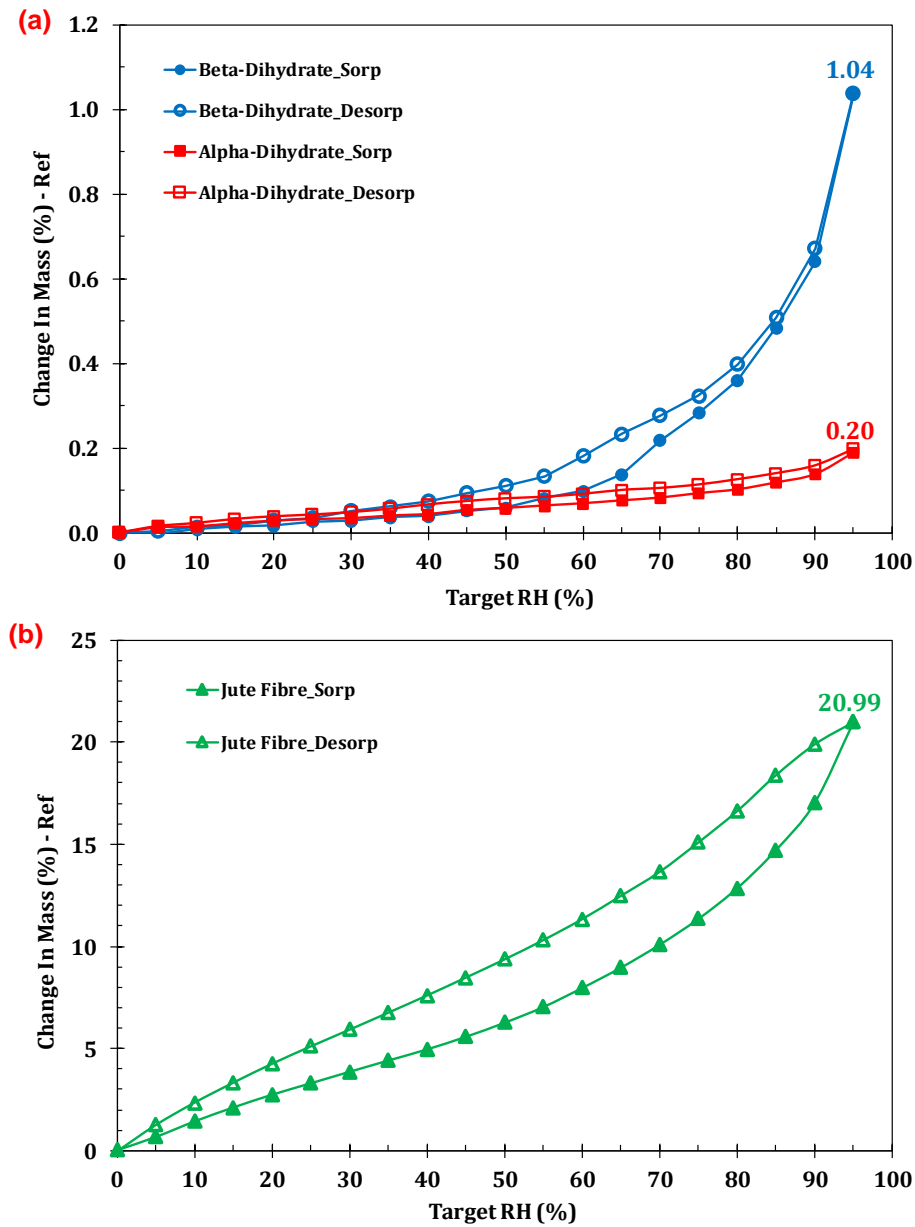


Figure 11 : Sorption and desorption isotherms of (a) alpha and beta gypsum dihydrate and (b) jute fibre

368

369 3.5 Fibre density

370 Canola oil is selected as the immersion liquid as it has been proven to give good
371 accuracy and repeatability for plant-based fibre density measurement [46]. In addition, it does
372 not impose health and safety risks, unlike benzene or other chemicals specified in the standard.
373 The density of store-bought canola oil was calculated as 0.9152 g/cm³ which is in agreement
374 with the value published in the literature [47]. The value is used to calculate the density of jute

fibres using Equation 3 and the results are given in Table 4. The measured density is an average of 5 specimens and the values are within the range of the published literature [11].

Table 4: Density of Jute Fibres

Hessian Sample	Measured Density (g/cm ³)	Literature Density (g/cm ³)
Loose Weave Hessian	1.4253	1.3 -1.5 [11]
Plain Weave Hessian	1.4709	
Historic Hessian	1.3743	

The variation in the above density measurement between different groups of jute fibres could be due to the complex structure of the fibre itself. The historic hessian is likely to have undergone chemical changes with time. Plant-based natural fibres are not uniform and fibre bundles containing ultimate fibres have irregular shapes. Each ultimate fibre has a complex, multi-layered cell wall and a central hollow lumen [11, 47]. The lumen area fraction for jute fibre is of the order of 34% which takes up significant proportion of the fibre cross-sectional area [11]. The actual size of lumen for jute and other plant-based fibres varies considerably depending on the source, age, treatment and separation technique [48]. Fidelis et.al. [49].measured the lumen size of jute fibre from Amazon (Brazil) as 6.7 µm in diameter while Ramesh et al.[50] reported the lumen size for jute obtained from India as 12 µm. Using the Archimedes method, it is possible that the the immersion liquid used might not completely fill up the tiny lumen which can lead to an inaccurate density measurement. A recommended technique for measuring fibre density is via helium gas pycnometry which is capable of producing repeatable and accurate data [46].

3.6 Single fibre bundle tensile properties

Table 5 presents the single fibre tensile strength of jute fibre bundles and their corresponding Weibull distribution parameters. A total of 20 fibre bundles were randomly chosen from a given batch and tested. The fibre bundle breaks at the weakest link, which can be anywhere along the fibre length. For example, the fibre bundle is likely to fail at the smallest cross-section area or at the most detrimental flaw such as at the site of cell wall buckling. The number of weak links increase with increasing fibre bundle length, causing the fibre bundle to be more susceptible to failure, resulting in lower strength[51].

Table 5 : Single fibre bundle tensile strength and Weibull distribution parameters

Properties	Loose Weave Hessian	Plain Weave Hessian	Historic Hessian
Fibre Bundle Cross-sectional Area (μm^2)	3471 \pm 3736	2641 \pm 1124	2447 \pm 877
Average Fibre Bundle Tensile Strength (MPa)	395 \pm 227	313 \pm 130	195 \pm 96
Scale Parameter, σ_o	457	352	220
Shape Parameter, m	1.66	2.48	2.54

The single fibre bundle tensile strength for loose weave hessian is found to be within the published data, ranging from 393 – 800 MPa [11] while the plain weave hessian exhibits a slightly lower mean fibre bundle strength. The fibre bundle strength of historic hessian is reduced significantly by 50% when compared to the 'as received' loose weave hessian, which indicates fibre degradation has occurred over time. Many authors [11, 48, 49] have pointed out that the large distribution of fibre bundle strengths in the published data can be related to the variability in the microstructure and chemical composition of the natural fibres. Other factors that have influence on fibre properties include, testing speed, gauge length, moisture content and temperature which are not always reported [11]. Nonetheless the current results are more comparable to the measured fibre bundle strengths reported by Defoirdt et al. [51] ranging from 307 \pm 84 MPa to 399 \pm 100 MPa. In a similar study, Fidelis et al. [49] published their single fibre bundle strengths as 314 \pm 131 MPa and 263 \pm 65 MPa for 20 mm and 30 mm gauge lengths respectively.

The Weibull distribution statistical analysis has been widely applied to describe the variability of single fibre bundle tensile strengths [49, 51-53]. The analysis relies on the assumption that the fibre bundle is brittle and its failure as a function of applied load is controlled by the most serious flaw (i.e. flaw subjected to the highest stress intensity factor) along the fibre length [53]. The two Weibull parameters that are of interest are (i) shape parameter (also known as Weibull modulus) m , a dimensionless parameter which defines the variability of the fibre failure strength and (ii) scale parameter, σ_o , which is a measure of characteristic strength and is dependent on the stress distribution and test specimen size.

Figure 12 shows the Weibull distribution for jute fibre tensile strengths from the present work. It can be seen from Figure 12(a), there is a good linear fit of the experimental data for

425 plain weave hessian fabric with the R^2 coefficient value more than 95%. However, this is not
 426 the case for the loose weave and historic hessian data which shows lack of fit with $R^2 \leq 95\%$.
 427 This is expected as there is often variation from linearity at the ends of the R^2 fitted line. The
 428 Weibull parameters m and σ_0 obtained from the gradient and intercept of the best fit lines of the
 429 graph are provided in Table 5. The Weibull modulus, m in this study was calculated as 1.66 and
 430 2.48 for the 'as received' loose weave and plain weave hessian fabrics respectively while m for
 431 historic hessian was calculated as 2.58. All of these values are within the range of the Weibull
 432 modulus for natural fibres which is between 1 and 6 [53]. The higher the m value as
 433 demonstrated by the plain weave and historic hessian fabrics indicates less variability in their
 434 tensile strength (i.e. narrow strength distribution). This is preferable as materials with high
 435 Weibull modulus are more predictable and less likely to break at a stress much lower than a
 436 mean value [31]. The characteristic strength, σ_0 for the 'as received' loose weave and plain
 437 weave hessian fabrics is 457 MPa and 352 MPa respectively which corresponds to the
 438 probability to failure, P_f of 63.2% as shown in Weibull cumulative probability plot (Figure 12(b)).
 439 As for the historic hessian, its σ_0 is 220 MPa, which is the lowest among the fabrics with the
 440 steepest curve gradient and the smallest range of strengths.

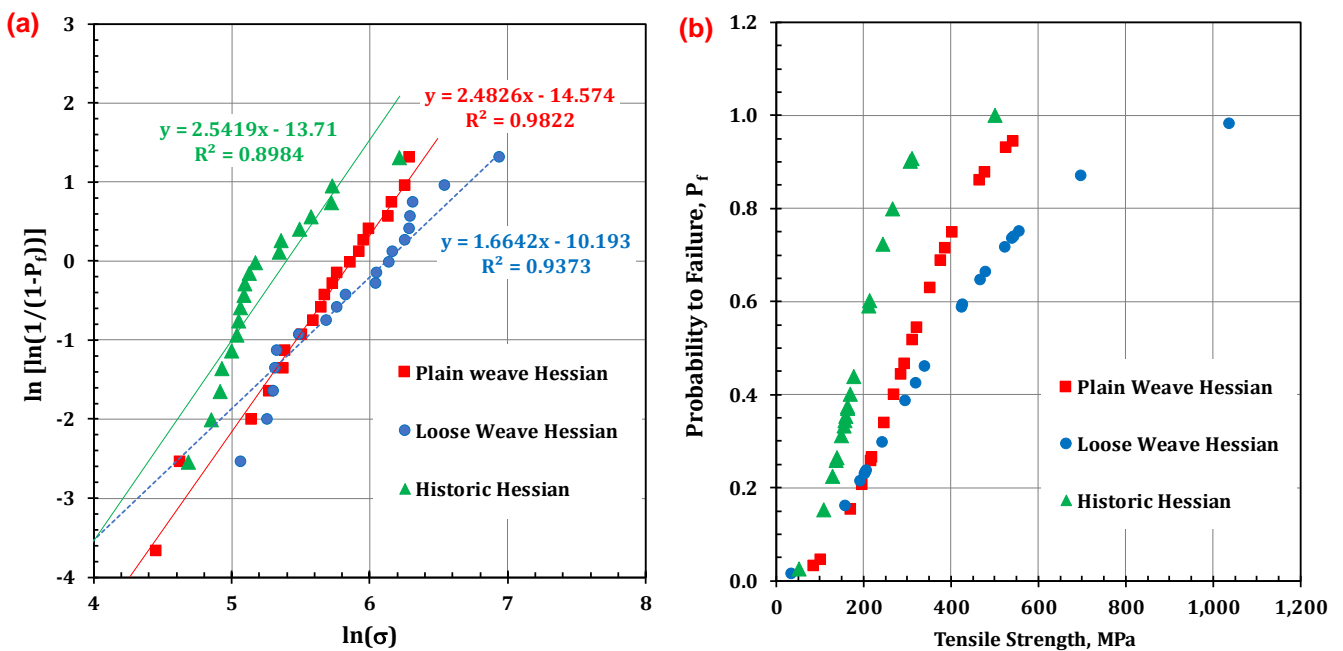


Figure 12: (a) Weibull plot and (b) Cumulative probability of failure from single fibre tensile strengths.

3.7 Flexural Strength and Modulus of Fibrous Plaster

Typical stress-strain curves for fibrous plaster specimens tested under flexural loading are shown in Figure 13. There are significant differences in the flexural behaviour of the gypsum plaster with and without reinforcement. The gypsum plasters without reinforcement (Figure 13(a)) failed catastrophically, characteristic of a brittle material where its maximum stress (σ_m) is the same as the breaking strength (σ_b) which resulted in the specimen being broken into two pieces. The incorporation of hessian reinforcement changed the flexural behaviour of the fibrous plaster as can be seen in Figure 13(b) where in this case, $\sigma_m > \sigma_b$. The failure occurred in a more controlled manner initiated by gypsum matrix cracking which then propagates and grows along the weak interface between the hessian and gypsum. This caused debonding of hessian fibres, and hence led to ultimate failure. It can be clearly seen in Figure 14(a) that the debonded hessian fibres (parallel to the specimen length) bridged the cracks and was capable of supporting reduced stress(~ 1 MPa). Similar behaviour was observed for fibrous plaster reinforced with quadaxial glass fibre in Figure 13(c), although in this case, matrix cracking and fibre debonding only occurred locally (see Figure 14(c)). The failed specimen is capable of holding a higher average stress of 3 MPa preventing the whole structure from failing catastrophically.

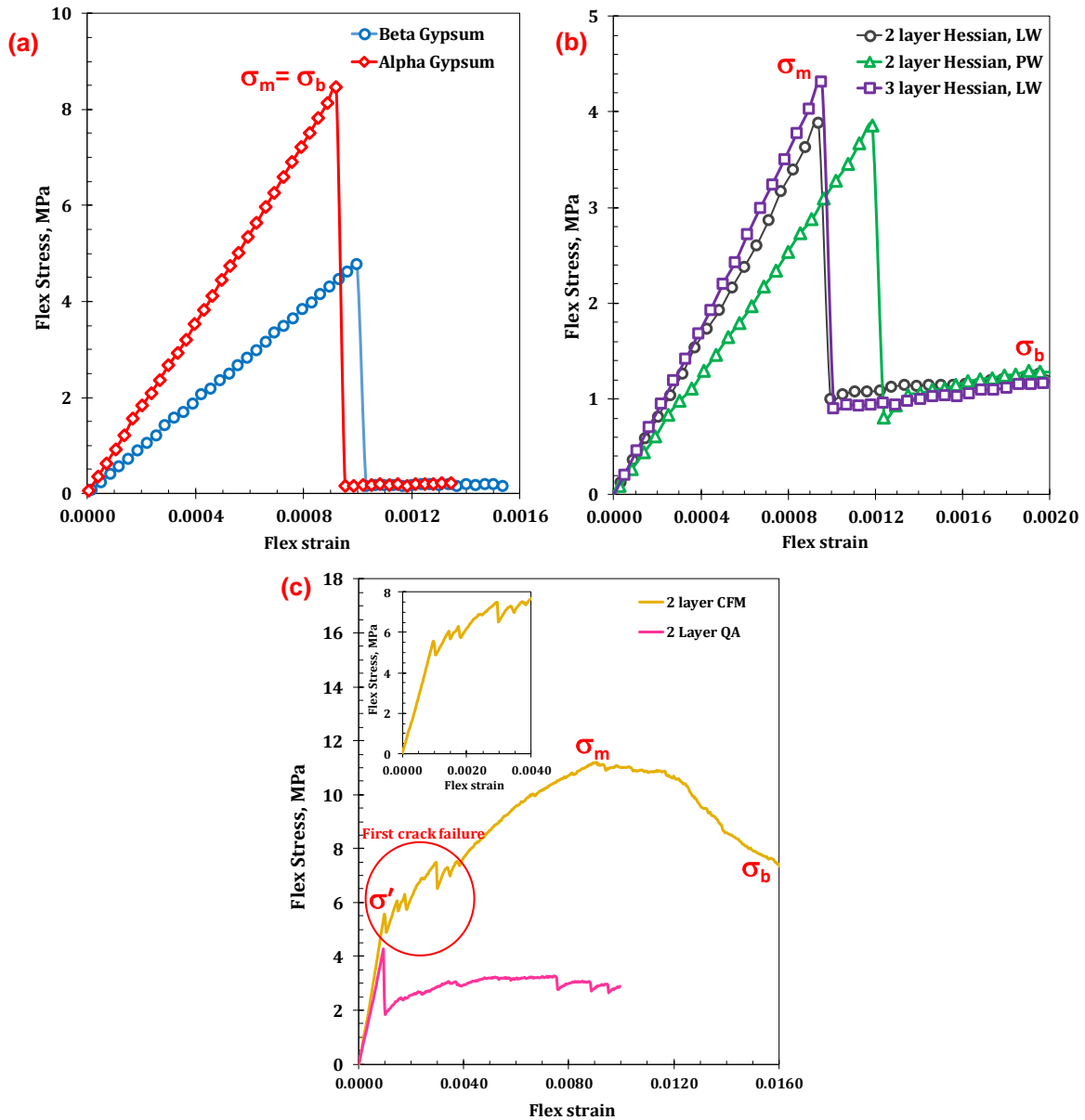


Figure 13: Stress-strain curves of flexural specimens (a) Gypsum without reinforcement - alpha and beta (b) Beta gypsum reinforced with hessian fibre (c) Beta gypsum reinforced with glass fibre
Inset picture showing first matrix cracking failure for gypsum reinforced with CFM

459

460 A different behaviour was demonstrated when the fibrous plaster was reinforced with

461 CFM, where the stress-strain curve in Figure 13(c) exhibited ductile behaviour. After initial

462 displacement, there was a sudden drop in the stress identified as σ' which is initiated by the

463 gypsum matrix cracking. The number of matrix cracks increased with increasing stress and

464 strain as demonstrated by the 'stick-slip' behaviour of the curve. The curve rose again as the

465 crack propagation in the structure was hindered by the strong fibre-gypsum interfacial adhesion,

466 until it reached the maximum strength (σ_m), after which the stress gradually decreased until

failure. Besides matrix cracking, other failure mode involves fibre debonding and pull-out (see Figure 14(b)) which occurred locally. It is worth mentioning that the specimens were still intact even after experiencing the whole failure sequence. The flexural strength and modulus of the fibrous plaster in this study are summarised in Table 6.

Table 6 : Flexural strength and modulus of fibrous plaster

Sample ID	Sample Description	Flexural Strength (MPa)	Flexural Modulus (GPa)
B-Gypsum	Beta Gypsum (BG) with no reinforcement	4.94 ± 0.27	4.54 ± 0.25
B+1H-LW	BG+ 1 layer of loose weave hessian	3.92	4.34
B+2H-LW	BG+ 2 layer of loose weave hessian	3.77 ± 0.52	3.97 ± 0.88
B+3H-LW	BG+ 3 layer of loose weave hessian	4.47 ± 1.07	4.26 ± 0.48
B+2 H-PW	BG+ 2 layer of plain weave hessian	3.48 ± 0.50	3.23 ± 0.48
A-Gypsum	Alpha Gypsum (AG) with no reinforcement	8.51 ± 0.90	8.24 ± 1.09
A+2H-LW	AG+ 2 layer of loose weave hessian	5.96 ± 0.67	6.49 ± 0.78
B_R+2H-LW	BG with sodium citrate retarding agent + 2 layer of loose weave hessian	3.36 ± 0.57	3.79 ± 0.83
B_RGS+2H-LW	BG with pearl glue retarding agent + 2 layer of loose weave hessian	2.54	3.43
B+2GF-CFM	BG + 2 layer of continuous fibreglass mat	4.57 ± 0.59^a 10.32 ± 1.09^b	4.93 ± 0.50^a
B+2GF-QA	BG + 2 layer of quadaxial glass fibre fabric	4.53 ± 0.44	3.90 ± 0.48

Note:

a:: Flexural strength and modulus corresponding to first matrix crack failure, σ'

b: Flexural strength corresponding to maximum load, σ_m

Broken test specimens showing a fractured surface of fibrous plaster under flexural loading are imaged in Figure 14. It can be clearly seen the debonded hessian fibre bundles (Figure 14(a)) and glass fibre yarns (Figure 14(b) and (c)) bridge the brittle crack in the gypsum plaster, preventing the structure from failing catastrophically. There is also evidence of extensive fibre debonding and pull-out.



Figure 14 : Broken test specimens showing fractured surface of fibrous plaster under flexural loading. (a) Fibrous plaster with hessian reinforcement (b) Fibrous plaster with continuous fibreglass mat (CFM) reinforcement (c) Fibrous plaster with quadaxial glass fibre reinforcement

3.7.1 Effect of Hessian Reinforcement on Flexural Properties of Fibrous plaster

The flexural strength of alpha and beta gypsum plasters without reinforcement were measured as 8.51 ± 0.90 MPa and 4.94 ± 0.27 MPa respectively. These experimental values fall within the range of values of autoclaved gypsum (7-10 MPa) and low-grade gypsum (4-5 MPa) reported in the literature [54]. The results agree well with our earlier observation in Section 3.3 that the beta gypsum has higher amount of pores (i.e. porosity) and larger threshold pore size than the alpha gypsum, thus contributing to its lower flexural strength. Figure 15 compares the effect of hessian reinforcement on the flexural strength of both gypsums.

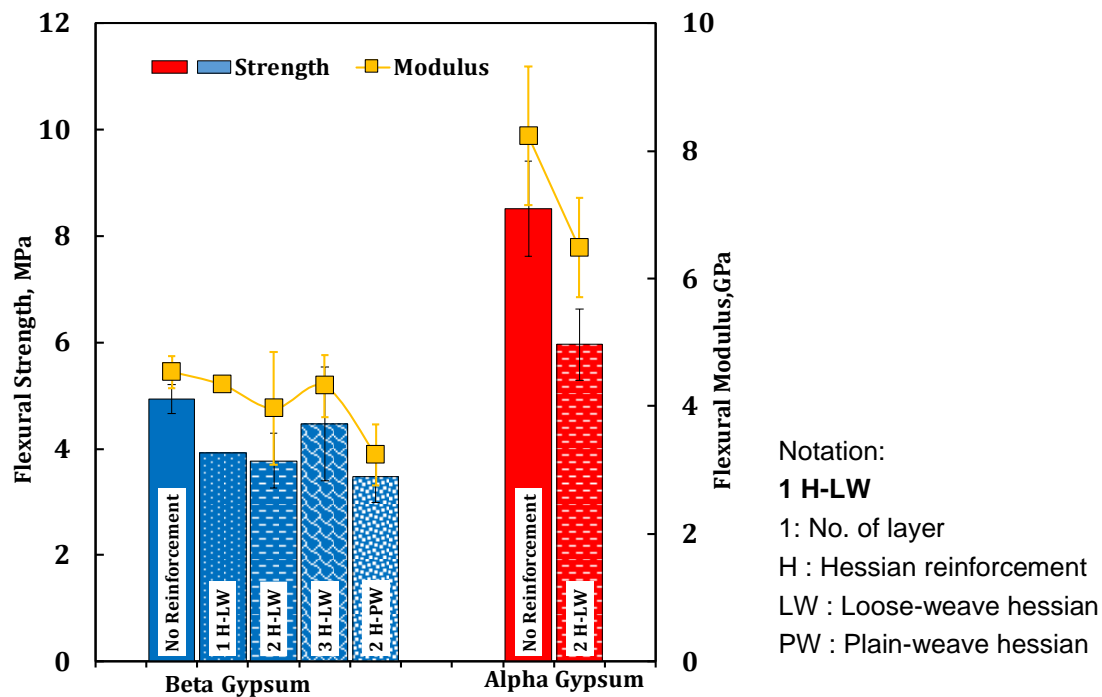


Figure 15 : Effect of hessian reinforcement on flexural properties of fibrous plaster.

It is evident that the addition of hessian reinforcement reduced the flexural strength quite remarkably, up to 30%. Similar trend is observed for the flexural modulus. Although the addition of 3 layers of hessian appears to improve the strength compared to samples with 1 or 2 layers, the improvement is very small and lies within the experimental error. Further tests are required to confirm whether or not 3 layers of hessian reinforcement would provide better fibrous plaster properties. The result also showed no marked difference when using loose weave and plain weave hessian which suggests the fibre architecture of hessian reinforcement has no effect on the overall flexural properties.

It is worth highlighting that the flexural strength reported here is determined by the fracture of the gypsum matrix which was the predominant failure of fibrous plaster flexural specimens. The addition of hessian reinforcement reduced the gypsum plaster volume fraction of the resulting composites and caused the structure to be less resistant to fracture. In addition, the presence of hessian reinforcement created flaws in the structure due to poor hessian-gypsum interfacial bonding. It can be concluded the combination of hessian and gypsum materials has no synergistic effect in improving the mechanical performance of fibrous plaster. The addition of hessian reinforcement is mainly to change or alter the failure behaviour of fibrous plaster by preventing catastrophic failure of gypsum, delaying crack propagation and

finally bridging the crack while supporting some part of the load. Hence the composite is more ductile and less likely to fail suddenly.

The detrimental effect of hessian reinforcement on fibrous plaster structure could be alleviated by carrying out fibre treatment either by physical, chemical or biological methods prior to the fabrication process. Depending on the method used, these treatments modify the fibre surface by increasing its polarity, removing unwanted fibre constituents such as lignin, pectin and hemicellulose or increasing surface roughness, all of which lead to an improve interfacial bond strength, as well as increasing moisture resistance of hessian fibres for better long term properties . Many studies [10, 17, 55] have demonstrated the positive effect of fibre treatment on the mechanical properties of natural fibre-gypsum composites

3.7.2 Effect of Glass Fibre Reinforcement on Flexural behaviour of Fibrous Plaster

Figure 16 compares the flexural properties of fibrous plaster reinforced with hessian and glass fibre. It is apparent that the fibrous plaster with glass fibre-reinforcement performs better than that of hessian-reinforced plaster. The flexural properties of CFM-reinforced gypsum plaster showed by far the biggest improvement exceeding the strength of the alpha gypsum with and without reinforcement. In addition, the use of CFM transformed the failure mode from brittle to ductile as well as increasing the strain to failure (displacement to failure.) Although the specimen experienced first crack failure corresponding to the failure mode of the gypsum, its load carrying capacity kept increasing until it reached maximum strength. The increase in strength is due to the strong interfacial glass fibre-gypsum bonding which contributes to better crack resistance and efficient load transfer in the structure.

On the other hand, the use of quadaxial glass fabric as the reinforcement in fibrous plaster did not improve the overall flexural strength as the specimen failed due to gypsum failure. Despite good fibre-gypsum interfacial bonding, the reinforcement effect was not observed due to lack of load transfer capability.

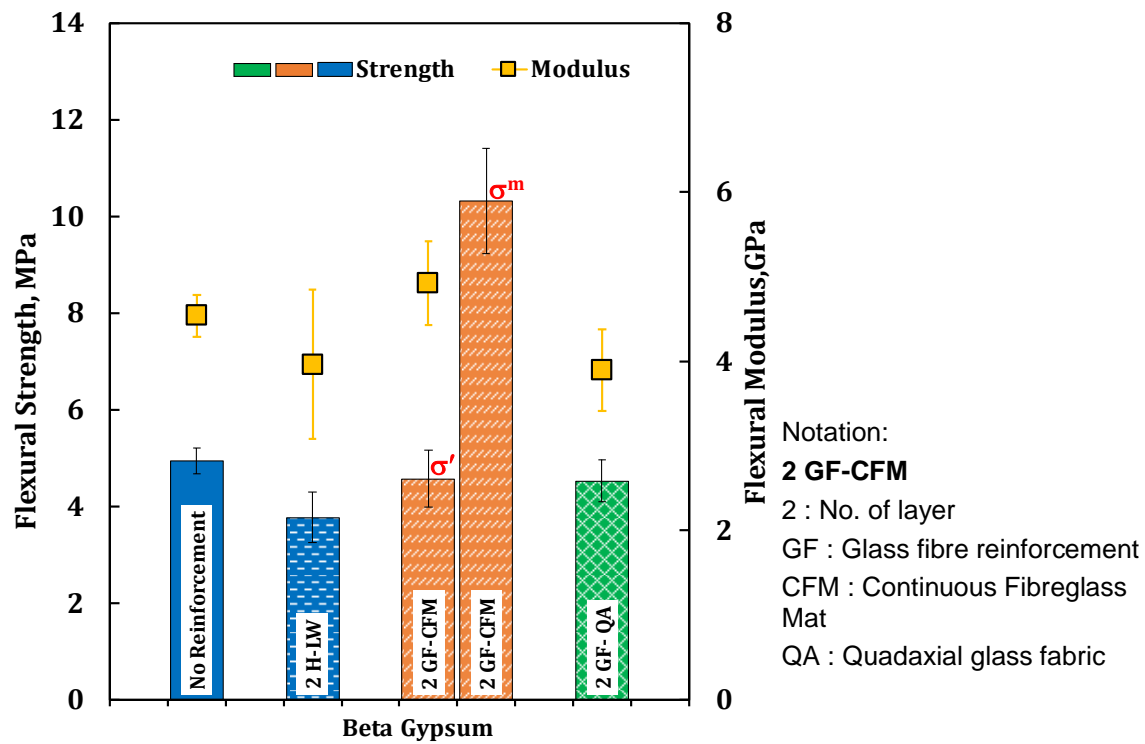


Figure 16 : Effect of glass fibre reinforcement on flexural properties of fibrous plaster. (σ' = Flex strength at first crack failure, σ_m = Maximum flex strength)

3.7.3 Effect of Retarder on Flexural Properties of Fibrous Plaster

Retarder is an additive which is added to the mixture in order to control and slow the setting time of gypsum plaster, thus prolonging its workability. Common retardants used with commercial gypsum include acids such as citric, malic, tartaric; ethyl acetate, potassium sulfate and polycarboxylic acids [56]. Citric acid has the highest retarding power while tartaric acid has the least power [8]. It can be clearly seen from Figure 17 that the addition of retarder reduced the flexural strength and modulus of fibre-reinforced gypsum. The strength dropped from 5 MPa to 3.4 MPa with the addition of sodium citrate retarder in sample Gypsum_R +2H. This value is also 11% lower than the strength of the specimen with the same configuration (Gypsum+2H). The addition of pearl glue retarder in sample Gypsum_RGS +2H further dropped the strength by 32%.

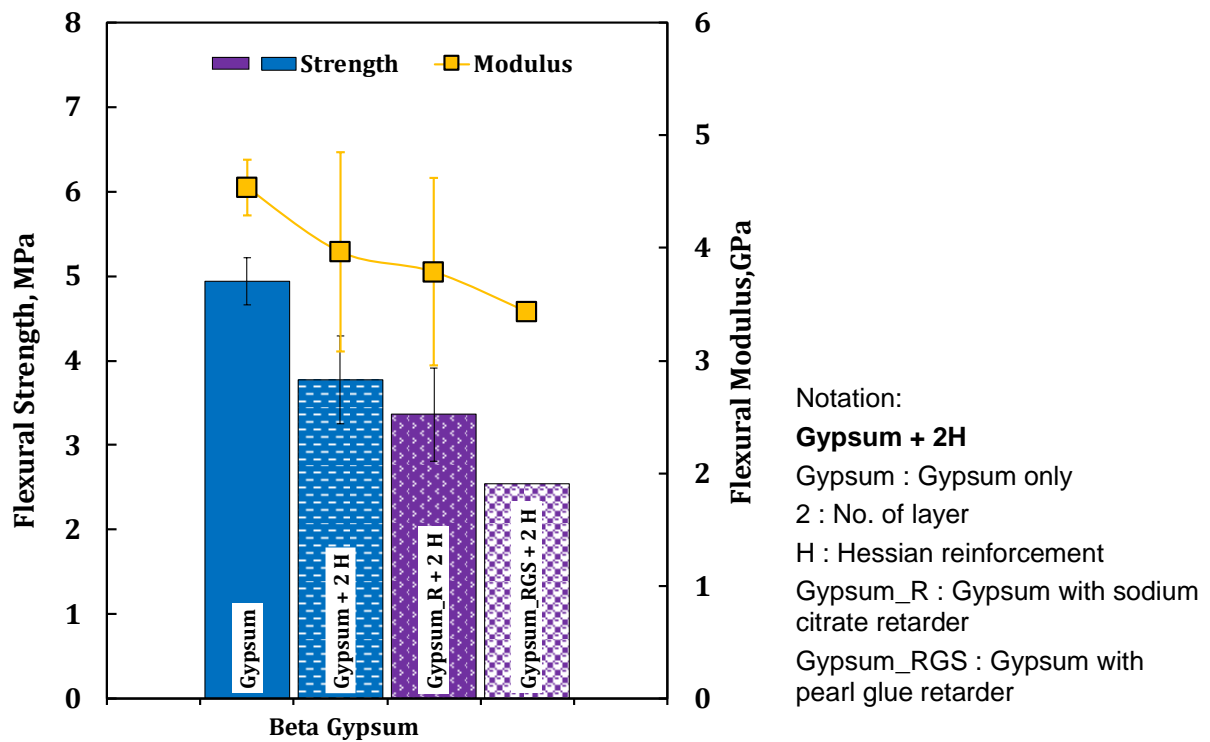


Figure 17: Effect of retarder on flexural properties of fibrous plaster

Although strength reductions were observed in the present work, these values can be considered small when compared to the work of Lanzon et al.[57] who observed more than 50% reduction in their gypsum samples when high concentrations of citric acid (1000 ppm and above) were added to the formulations. The addition of citric acid at low concentrations (500 ppm and below) on the other hand, had negligible effect on the strength.

The reduction in mechanical properties of gypsum plaster due to the presence of retarder can be explained in terms of microstructural changes. The final strength of gypsum is related to the formation of needle shaped gypsum crystals with a high degree of interlocking which takes place during the hydration process. The addition of retarder modifies the nucleation and the crystal growth process as the acids are absorbed at the crystal surfaces of the growing gypsum thereby lowering the degree of interlocking and reducing the force of adhesion between different faces of the gypsum crystals [8]. The difference in the gypsum microstructure with high and low degrees of interlocking can be seen in Lanzon et al.[57]. In this study, the microstructural differences between gypsum with and without retarder are not obvious due to the fact that only low concentrations of retarders were used (to reflect industry practice) in the mixture which resulted in fairly small strength reductions.

3.8 Microstructural Observation

Figure 18 shows the image of fractured jute fibre bundles encrusted with gypsum crystals on their surfaces. The fibre bundles contains about seven ultimate fibres, each of which has a central void or lumen.

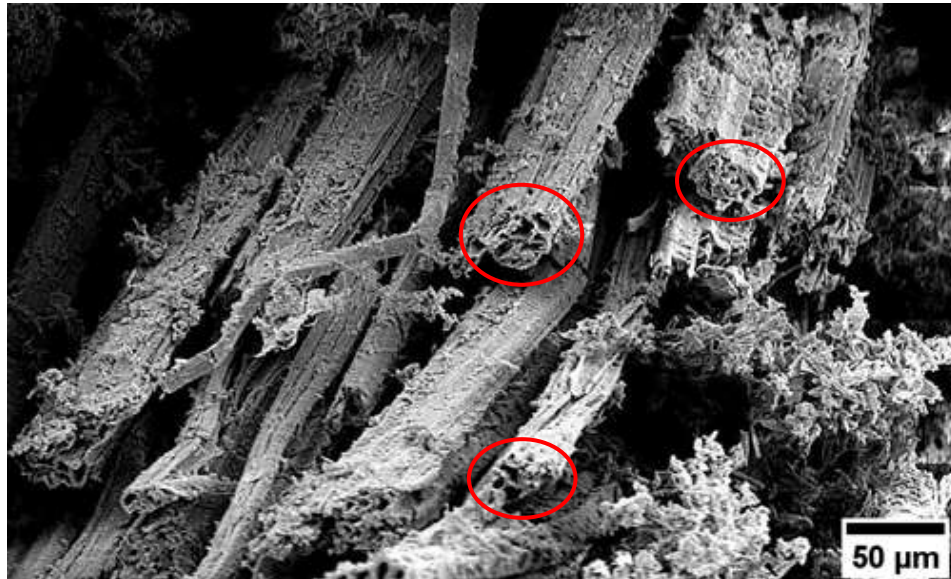


Figure 18: Lumens in jute fibre bundles as circled

Low magnification (x100) images of the smooth and fractured surfaces of beta gypsum plasters are presented in Figure 19(a) and (b). The fractured surface contains spherical pores. The smooth surface is comprised of a network of needle shaped crystals of gypsum dihydrate with micropores in between (Figure 19 (c)). The alpha gypsum plaster has a more disorganised microstructure (Figure 19 (d)) with less coarse porosity (dark zones), some flattened zones and polymer strands evident.

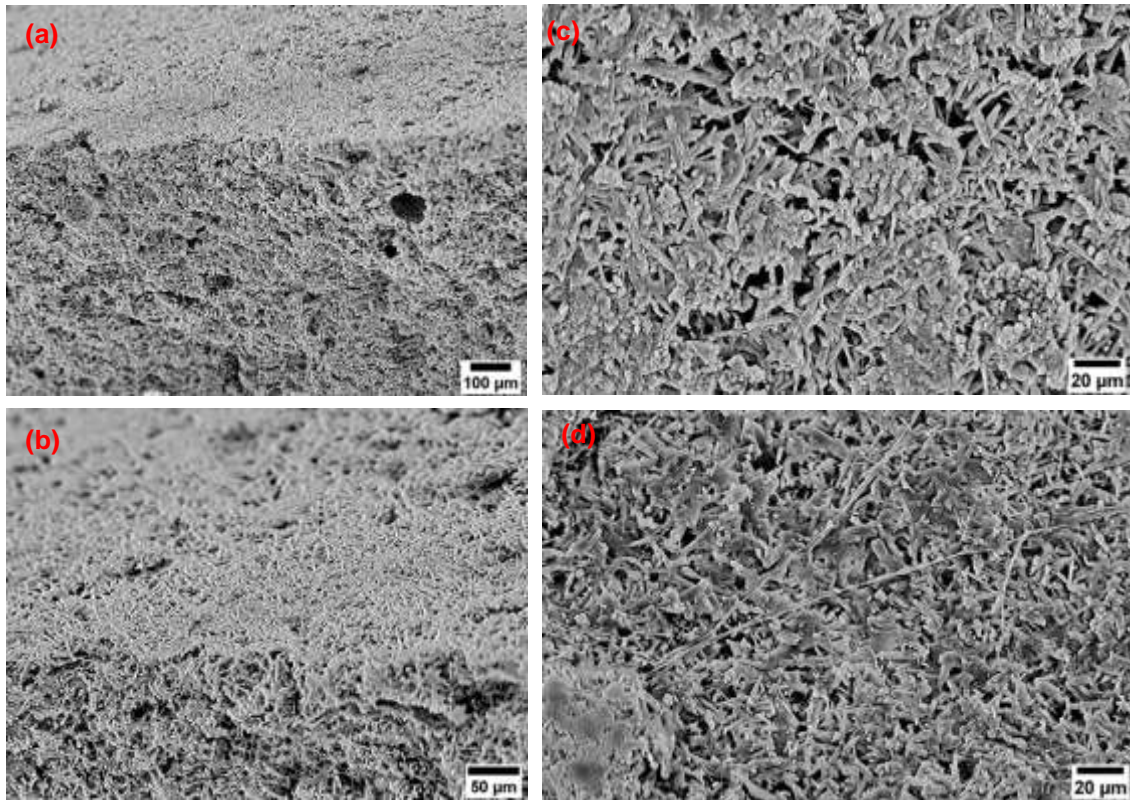


Figure 19 : Edge view of fractured sheet of beta gypsum plaster with smooth face (upper) and rougher, porous fractured surface (lower) at x100 (a) and x250 (b). Smooth surface of beta gypsum plaster x500 (c) and alpha gypsum plaster x500 (d)

574

575 The fractured surfaces of the alpha and beta gypsum plasters are imaged in Figure 20.

576 Both plasters containing spherical pores, some of which are charged (white zones).

577 Examination of the interior of the pores reveals a less closely packed structure in the beta

578 plaster (Figure 20(c)) compared to the alpha plaster (Figure 20(d)).

579

580

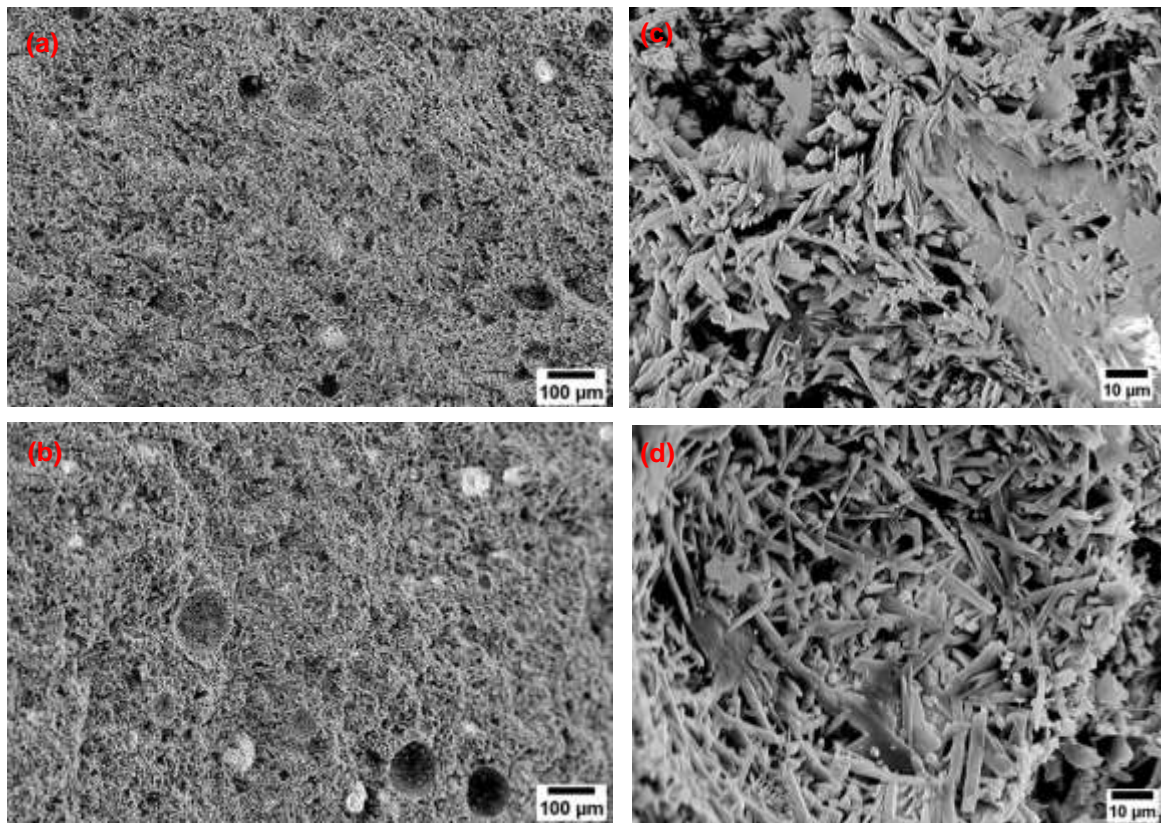


Figure 20 : Fracture surfaces of beta plaster (a) and alpha plaster (b), both x100. Fracture surfaces of pores in (c) beta gypsum plaster and (d) alpha gypsum plaster both x1,000.

It can be concluded that the microstructures of the alpha and beta gypsum plasters are not substantially different and both are comprised of calcium dihydrate needle crystals. The needle crystals are more closely packed and interconnected in the strong plaster and there are therefore more stress raisers in the ordinary plaster which is expected to be weaker. Both alpha and beta plasters contain porosity but the calcium dihydrate crystals are more closely packed in the alpha plaster. There are fine strands of polymer within the alpha plaster which may be a prescribed ingredient and may contribute to its superior strength. The mean density of the beta plaster was measured to be 1060 kg.m^{-3} and the mean density of the alpha plaster was measured to be 1350 kg.m^{-3} supporting the above observations.

4. Conclusions

This study investigated the structural performance of fibrous plaster containing different numbers of layers of hessian and glass fibre reinforcements. Based on this investigation, the fibrous plaster with glass fibre-reinforcement particularly the continuous fibreglass mat reinforcement, performs exceptionally well compared with hessian reinforcement. The glass

fibre-reinforced gypsum plaster exceeds the flexural strength of the alpha gypsum plaster without reinforcement as well as transforming the failure mode from brittle to ductile. The improvement is due to the strong interfacial bonding between the materials which contributes to better crack resistance and efficient load transfer in the structure. Although the use of hessian reinforcement with gypsum plaster did not influence the flexural strength, the presence of the hessian is still beneficial in preventing catastrophic failure of gypsum, delaying crack propagation and subsequent bridging of the crack. To improve the mechanical performance of the hessian reinforced gypsum plaster, the hessian reinforcement might benefit from surface chemical treatment in order to raise the interfacial strength.

The outcomes of this work will provide essential data serving as the basis for the development of further materials research in predicting the durability and life span of fibrous plaster structures. The mechanical properties and failure mechanisms identified in this study will provide a better understanding of failure and improve specification of conservation repairs which are currently based on empirical experience and not scientific evidence. This first stage of testing has compared the physical and mechanical properties of modern fibrous plasters, but does not include recommendations for the repair of historic fibrous plasterwork. The choice of materials for conservation is far more nuanced, taking into account the overall structure of composite ceilings, the condition of historic materials and compatibility of repairs with them. Further materials research is needed to understand this neglected historic material.

5. Future Work

The findings presented in this paper will be developed to further the understanding of fibrous plaster degradation and how this is affected by environmental conditions. Building upon this, the use of modern materials in the maintenance and repair of historic fibrous plaster will also be addressed along with strategies and methods to predict the properties and failure of historic plaster currently in service. Our ongoing studies will include a series of publications where an investigation of the load bearing capacity and failure mechanisms of fibrous plaster wads, used to suspend fibrous plaster ceilings directly below a loadbearing roof structure, is presented in Part 2 and, the durability and degradation of hessian and glass fibre reinforced gypsum composites are presented in Part 3.

6. Acknowledgements

The research work is supported by Historic England and the University of Bath. The authors gratefully acknowledge Mr John Vallender, Historic England artist, for his illustration work of fibrous plaster in Figure 3. The authors would also like to thank Mr. Nutchanon Tantiboon for his work on fibre density measurements and single fibre bundle tensile tests and Dr Olivier Camus for carrying out the Mercury Intrusion Porosimeter experiment. We also thank Mr William Bazely and Mr Neil Price for providing technical support during the course of this work

7. References

- [1] Historic England. *Historic Fibrous Plaster in the UK: Guidance on its Care and Management*. 2019; Available from: <https://historicengland.org.uk/images-books/publications/historic-fibrous-plaster/heag269-historic-fibrous-plaster/>.
- [2] G. Beard, J. Orton, R. Ireland, *Decorative Plasterwork in Great Britain*, Routledge 2015 (Original work published 1975).
- [3] C. Barrett, *The Effects of Moisture and Acoustic Degradation on Fibrous Plaster Panel Ceilings*, Department of Architecture and Civil Engineering, University of Bath, Bath, 2019,
- [4] The Gazette. *Another gig postponed as Blackpool's Empress Ballroom repair gets underway*. 14 September 2017 27 September 2017 [cited 2020 03 June]; Available from: <https://www.blackpoolgazette.co.uk/news/another-gig-postponed-blackpools-empress-ballroom-repair-gets-underway-840355>.
- [5] The Telegraph. *Savoy ceiling collapses during auction for Princess Anne's former school*. March 2019 [cited 2020 27 May]; Available from: <https://www.telegraph.co.uk/news/2019/03/04/savoy-ceiling-collapses-auction-princess-annes-former-school/>.
- [6] A. Coburn, E. Dudley, R. Spence, *Gypsum Plaster*, Intermediate Technology Publications, January 1989 (Original work published).
- [7] F. Wirsching, Calcium Sulfate, *Ullmann's Encyclopedia of Industrial Chemistry*, (Ed.), Wiley-VCH Verlag GmbH & Co. KGaA2000.
- [8] N.B. Singh, B. Middendorf, Calcium sulphate hemihydrate hydration leading to gypsum crystallization, *Progress in Crystal Growth and Characterization of Materials* 53(1) (2007) 57-77 DOI: 10.1016/j.pcrysgrow.2007.01.002.
- [9] M.A. Ali, F.J. Grimer, Mechanical Properties of Glass Fibre-Reinforced Gypsum, *Journal of Materials Science* 4(5) (1969) 389-& DOI: Doi 10.1007/Bf00549703.
- [10] F. Iucolano, D. Caputo, F. Leboffe, B. Liguori, Mechanical behavior of plaster reinforced with abaca fibers, *Construction and Building Materials* 99 (2015) 184-191 DOI: 10.1016/j.conbuildmat.2015.09.020.
- [11] K.L. Pickering, M.G.A. Efendy, T.M. Le, A review of recent developments in natural fibre composites and their mechanical performance, *Compos Part a-Appl S* 83 (2016) 98-112 DOI: 10.1016/j.compositesa.2015.08.038.
- [12] M. Ramesh, K. Palanikumar, K.H. Reddy, Plant fibre based bio-composites: Sustainable and renewable green materials, *Renew Sust Energ Rev* 79 (2017) 558-584 DOI: 10.1016/j.rser.2017.05.094.
- [13] S.K. Ramamoorthy, M. Skrifvars, A. Persson, A Review of Natural Fibers Used in Biocomposites: Plant, Animal and Regenerated Cellulose Fibers, *Polymer Reviews* 55(1) (2015) 107-162 DOI: 10.1080/15583724.2014.971124.
- [14] Premier Plaster Moulding. *Glass Reinforced Gypsum (GRG)*. [Online] 2019 20-11-2019]; Available from: <https://www.premierplastermouldings.com/contact-premier-plaster-mouldings-northern-ireland/>.
- [15] Stromberg. *Stromberg GFRG*. [Online] 2012 20-11-2019]; Available from: <https://www.strombergarchitectural.com/materials/gfrg>.
- [16] Y.F. Wu, The effect of longitudinal reinforcement on the cyclic shear behavior of glass fiber reinforced gypsum wall panels: tests, *Engineering Structures* 26(11) (2004) 1633-1646 DOI: 10.1016/j.engstruct.2004.06.009.

- [17] F. Iucolano, L. Boccarusso, A. Langella, Hemp as eco-friendly substitute of glass fibres for gypsum reinforcement: Impact and flexural behaviour, *Compos Part B-Eng* 175 (2019) 107073 DOI: 10.1016/j.compositesb.2019.107073.
- [18] S. Eve, M. Gomina, A. Gmouh, A. Samdi, R. Moussa, G. Orange, Microstructural and mechanical behaviour of polyamide fibre-reinforced plaster composites, *Journal of the European Ceramic Society* 22(13) (2002) 2269-2275 DOI: Doi 10.1016/S0955-2219(02)00014-6.
- [19] C. Zhu, J.X. Zhang, J.H. Peng, W.X. Cao, J.S. Liu, Physical and mechanical properties of gypsum-based composites reinforced with PVA and PP fibers, *Construction and Building Materials* 163 (2018) 695-705 DOI: 10.1016/j.conbuildmat.2017.12.168.
- [20] A.J. Lewry, J. Williamson, The setting of gypsum plaster, *Journal of Materials Science* 29(20) (1994) 5279-5284 DOI: 10.1007/bf01171536.
- [21] Industrial Plasters Ltd. *Prestia Creation Plaster*. 2020; Available from: <http://www.industrialplasters.com/prod/prestia-casting-plaster/prestia-creation-plaster-1>.
- [22] Industrial Plasters Ltd. *Prestia Classic Plaster*. 2020; Available from: <http://www.industrialplasters.com/prod/prestia-casting-plaster/prestia-classic-plaster-1>.
- [23] Industrial Plasters Ltd. *Unifilo U816 CFM Fibreglass Mat (225g)*. 2020; Available from: <http://www.industrialplasters.com/prod/resin-fibreglass/unifilo-u816-cfm-fibreglass-mat-225g-1>.
- [24] Jesmonite Ltd., AR Quadaxial Glass, Technical Data Sheet, n.d,
- [25] Jesmonite Ltd. *Products - Additive and Reinforcement*. [Online] n.d; Available from: <https://jesmonite.com/products/additives-and-reinforcements/>.
- [26] Z.Y. Gao, Q.H. Hu, Estimating permeability using median pore-throat radius obtained from mercury intrusion porosimetry, *Journal of Geophysics and Engineering* 10(2) (2013) DOI: 10.1088/1742-2132/10/2/025014.
- [27] Surface Measurement Systems Ltd., DVS Intrinsic - Compact and Economical Dynamic Vapor Sorption System, nd,
- [28] British Standards Institute, Carbon Fibre - Determination of density, BS ISO 10119:2002, BSI, London, 2002,
- [29] British Standards Institute, Plastics - Liquid resins - Determination of density by the pycnometer method, BS EN ISO 1675:1998, BSI, London, 1998,
- [30] British Standards Institute, Carbon Fibre - Determination of the tensile properties of single-filament specimens, BS ISO 11566 : 1996, BSI, London, 1996,
- [31] J.B. Quinn, G.D. Quinn, A practical and systematic review of Weibull statistics for reporting strengths of dental materials, *Dent Mater* 26(2) (2010) 135-47 DOI: 10.1016/j.dental.2009.09.006.
- [32] British Standards Institute, Plastics - Determination of flexural properties, BS EN ISO 178 : 2010+A1:2013, BSI, London, 2013,
- [33] F. Iucolano, B. Liguori, P. Aprea, D. Caputo, Thermo-mechanical behaviour of hemp fibers-reinforced gypsum plasters, *Construction and Building Materials* 185 (2018) 256-263 DOI: 10.1016/j.conbuildmat.2018.07.036.
- [34] E. Romero, P.H. Simms, Microstructure Investigation in Unsaturated Soils: A Review with Special Attention to Contribution of Mercury Intrusion Porosimetry and Environmental Scanning Electron Microscopy, *Geotechnical and Geological Engineering* 26(6) (2008) 705-727 DOI: 10.1007/s10706-008-9204-5.
- [35] S. Maria, Methods for porosity measurement in lime-based mortars, *Construction and Building Materials* 24(12) (2010) 2572-2578 DOI: 10.1016/j.conbuildmat.2010.05.019.

- [36] H.Y. Ma, Mercury intrusion porosimetry in concrete technology: tips in measurement, pore structure parameter acquisition and application, *Journal of Porous Materials* 21(2) (2014) 207-215 DOI: 10.1007/s10934-013-9765-4.
- [37] L. Cui, J.H. Cahyadi, Permeability and pore structure of OPC paste, *Cement and Concrete Research* 31(2) (2001) 277-282 DOI: Doi 10.1016/S0008-8846(00)00474-9.
- [38] N. Alderete, Y. Villagran, A. Mignon, D. Snoeck, N. De Belie, Pore structure description of mortars containing ground granulated blast-furnace slag by mercury intrusion porosimetry and dynamic vapour sorption, *Construction and Building Materials* 145 (2017) 157-165 DOI: 10.1016/j.conbuildmat.2017.03.245.
- [39] M.M.C. Canut, Pore Structure in Blended Cement Paste, Department of Civil Engineering, Technical University of Denmark, Lyngby, Denmark, 2012, p. 346
- [40] S. Diamond, Mercury porosimetry - An inappropriate method for the measurement of pore size distributions in cement-based materials, *Cement and Concrete Research* 30(10) (2000) 1517-1525 DOI: Doi 10.1016/S0008-8846(00)00370-7.
- [41] F. Collet, J. Chamoin, S. Pretot, C. Lanos, Comparison of the hygric behaviour of three hemp concretes, *Energy and Buildings* 62 (2013) 294-303 DOI: 10.1016/j.enbuild.2013.03.010.
- [42] M. Karoglou, A. Moropoulou, Z.B. Maroulis, M.K. Krokida, Water sorption isotherms of some building materials, *Drying Technology* 23(1-2) (2005) 289-303 DOI: 10.1081/Drt-200047948.
- [43] M. Thommes, K. Kaneko, A.V. Neimark, J.P. Olivier, F. Rodriguez-Reinoso, J. Rouquerol, K.S.W. Sing, Physisorption of gases, with special reference to the evaluation of surface area and pore size distribution (IUPAC Technical Report), *Pure and Applied Chemistry* 87(9-10) (2015) 1051-1069 DOI: 10.1515/pac-2014-1117.
- [44] M.A. Sawpan, K.L. Pickering, A. Fernyhough, Effect of various chemical treatments on the fibre structure and tensile properties of industrial hemp fibres, *Compos Part a-Appl S* 42(8) (2011) 888-895 DOI: 10.1016/j.compositesa.2011.03.008.
- [45] C.A.S. Hill, A. Norton, G. Newman, The Water Vapor Sorption Behavior of Natural Fibers, *Journal of Applied Polymer Science* 112(3) (2009) 1524-1537 DOI: 10.1002/app.29725.
- [46] M. Truong, W. Zhong, S. Boyko, M. Alcock, A comparative study on natural fibre density measurement, *J Text I* 100(6) (2009) 525-529 DOI: 10.1080/00405000801997595.
- [47] A. Amiri, Z. Triplett, A. Moreira, N. Brezinka, M. Alcock, C.A. Ulven, Standard density measurement method development for flax fiber, *Industrial Crops and Products* 96 (2017) 196-202 DOI: 10.1016/j.indcrop.2016.11.060.
- [48] A.K. Mohanty, M. Misra, L.T. Drzal, Surface modifications of natural fibers and performance of the resulting biocomposites: An overview, *Composite Interfaces* 8(5) (2001) 313-343 DOI: Doi 10.1163/156855401753255422.
- [49] M.E. Alves Fidelis, T.V.C. Pereira, O.d.F.M. Gomes, F. de Andrade Silva, R.D. Toledo Filho, The effect of fiber morphology on the tensile strength of natural fibers, *Journal of Materials Research and Technology* 2(2) (2013) 149-157 DOI: 10.1016/j.jmrt.2013.02.003.
- [50] M. Ramesh, K. Palanikumar, K.H. Reddy, Mechanical property evaluation of sisal-jute-glass fiber reinforced polyester composites, *Composites Part B: Engineering* 48 (2013) 1-9 DOI: 10.1016/j.compositesb.2012.12.004.
- [51] N. Defoirdt, S. Biswas, L. De Vriese, L.Q.N. Tran, J. Van Acker, Q. Ahsan, L. Gorbatikh, A. Van Vuure, I. Verpoest, Assessment of the tensile properties of coir, bamboo and jute fibre, *Compos Part a-Appl S* 41(5) (2010) 588-595 DOI: 10.1016/j.compositesa.2010.01.005.

- [52] Z.P. Xia, J.Y. Yu, L.D. Cheng, L.F. Liu, W.M. Wang, Study on the breaking strength of jute fibres using modified Weibull distribution, *Compos Part a-Appl S* 40(1) (2009) 54-59 DOI: 10.1016/j.compositesa.2008.10.001.
- [53] E. Trujillo, M. Moesen, L. Osorio, A.W. Van Vuure, J. Ivens, I. Verpoest, Bamboo fibres for reinforcement in composite materials: Strength Weibull analysis, *Compos Part a-Appl S* 61 (2014) 115-125 DOI: 10.1016/j.compositesa.2014.02.003.
- [54] M. Singh, M. Garg, Gypsum-based fibre-reinforced composites: an alternative to timber, *Construction and Building Materials* 8(3) (1994) 155-160 DOI: 10.1016/s0950-0618(09)90028-9.
- [55] P. Dalmay, A. Smith, T. Chotard, P. Sahay-Turner, V. Gloaguen, P. Krausz, Properties of cellulosic fibre reinforced plaster: influence of hemp or flax fibres on the properties of set gypsum, *Journal of Materials Science* 45(3) (2010) 793-803 DOI: 10.1007/s10853-009-4002-x.
- [56] G. Camarini, M.C.C. Pinto, A.G. de Moura, N.R. Manzo, Effect of citric acid on properties of recycled gypsum plaster to building components, *Construction and Building Materials* 124 (2016) 383-390 DOI: 10.1016/j.conbuildmat.2016.07.112.
- [57] M. Lanzon, P.A. Garcia-Ruiz, Effect of citric acid on setting inhibition and mechanical properties of gypsum building plasters, *Construction and Building Materials* 28(1) (2012) 506-511 DOI: 10.1016/j.conbuildmat.2011.06.072.